Coordination Chemistry Reviews 364 (2018) 33–50

Contents lists available at ScienceDirect

Coordination Chemistry Reviews

journal homepage: www.elsevier.com/locate/ccr

Review

Designing bipyridine-functionalized zirconium metal–organic frameworks as a platform for clean energy and other emerging applications

Thach N. Tu [a,b], My V. Nguyen [a,c], Ha L. Nguyen [a,d], Brian Yuliarto [e], Kyle E. Cordova [d,f], Selçuk Demir [g,*]

[a] Vietnam National University-Ho Chi Minh City (VNU-HCM), Ho Chi Minh 721337, Viet Nam
[b] Bach Khoa University, VNU-HCM, Ho Chi Minh 721337, Viet Nam
[c] University of Science, VNU-HCM, Ho Chi Minh 721337, Viet Nam
[d] Center for Research Excellence in Nanotechnology, King Fahd University of Petroleum and Minerals, Dhahran 31261, Saudi Arabia
[e] Research Center of Nanosciences and Nanotechnology, Institut Teknologi Bandung, Bandung 40132, Indonesia
[f] Berkeley Global Science Institute, University of California, Berkeley, Berkeley, CA 94720, USA
[g] Department of Chemistry, Faculty of Arts and Sciences, Recep Tayyip Erdogan University, Rize 53100, Turkey

ARTICLE INFO

Article history:
Received 26 December 2017
Accepted 11 March 2018

Keywords:
Metal–organic frameworks
Reticular chemistry
Porous materials
Heterogeneous catalysis
Clean energy
Hydrogen production
Solar fuels
Solar cell materials

ABSTRACT

Metal–organic frameworks (MOFs) are a class of crystalline and porous materials with modular structural features. This modularity has allowed MOFs to be designed and synthesized with adjustable pore sizes and shapes leading to ultrahigh porosity. Among the tens of thousands of known MOF structures, zirconium-based MOFs (Zr-MOFs) have attracted attention not only for their structural properties but also their superior chemical and thermal stabilities, which are critical for a myriad of practical applications. In particular, bipyridine (BPY) functionalized Zr-MOFs have been received recognition for their interesting intrinsic properties, which arise from various post-modification pathways. The fact that post-modification is readily available for such MOFs paves the way towards anchoring specific components (functional groups, metals complexes, and nanoparticles) via the bipyridine docking centers, thus endowing this MOF platform with the capability to chemically alter and enhance the bulk material's properties. Throughout this review, an emphasis is placed on the preparation of BPY-functionalized Zr-MOFs, their characterization, and subsequent applications, such as electrocatalytic or photocatalytic hydrogen evolution reactions, heterogeneous molecular catalysis, and gas storage for renewable energy. Furthermore, this review highlights the design and applications of materials from the viewpoint of materials design and the necessity and importance of installing complexity to achieve synergistic interactions. Finally, our perspective for future applications is introduced with the expectation of providing useful information to those interested in this specific MOF platform.

Contents

* Corresponding author.
E-mail address: selcuk.demir@erdogan.edu.tr (S. Demir).

https://doi.org/10.1016/j.ccr.2018.03.014
0010-8545/

1. Introduction

Metal–organic frameworks (MOFs), a new generation of highly advanced porous materials, provide a platform for solving global environmental problems. The beauty of MOF materials, which are governed by the principles of reticular chemistry, lies in the fact that the proper selection of constituent building blocks results in designable crystal structures owning adjustable pore sizes and shapes, and tunable internal chemical environments [1]. These features have endowed MOFs with the ability to be applied to a range of applications, including gas storage and separation [2,3], catalysis [4], drug delivery [5], proton conducting applications [6,7], and molecular sensing [8]. Recently, zirconium-based MOFs (Zr-MOFs) have gained much interest not only due to their high thermal and chemical stability, which are vastly superior to other known MOFs, but also because of their performance in a variety of applications, including catalysis and clean energy (Fig. 1) [9–13]. Together with the advances in the synthesis of new MOF materials [14–17] adopting diverse topologies [18–23], significant efforts have focused on decorating and post-synthetically functionalizing the interior surface of Zr-MOFs for enhancing their performance in specific, novel applications. Among these, bipyridine-functionalized (BPY) Zr-MOFs have stood out primarily due to the ability to modify their structures through various post-synthetic modification pathways in order to anchor specific components (functional groups, metal complexes, nanoparticles) via

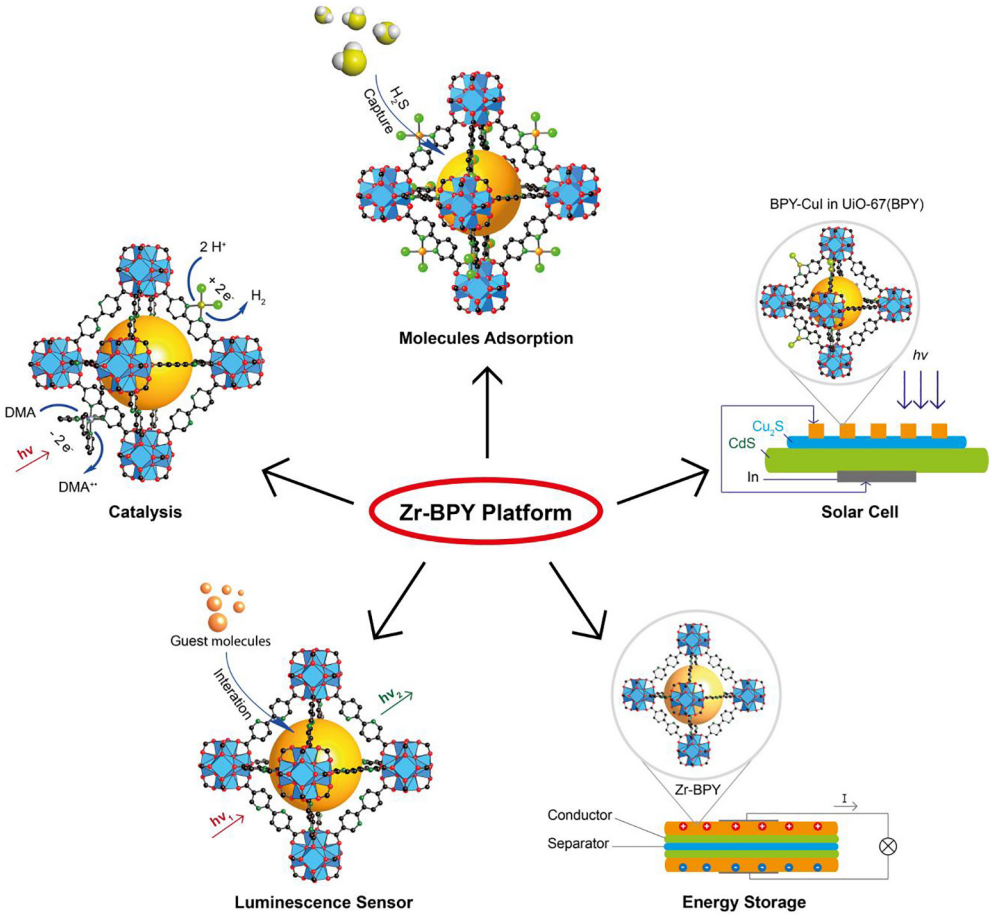

Fig. 1. Schematic illustration of different pathways toward applications of UiO-67(BPY).

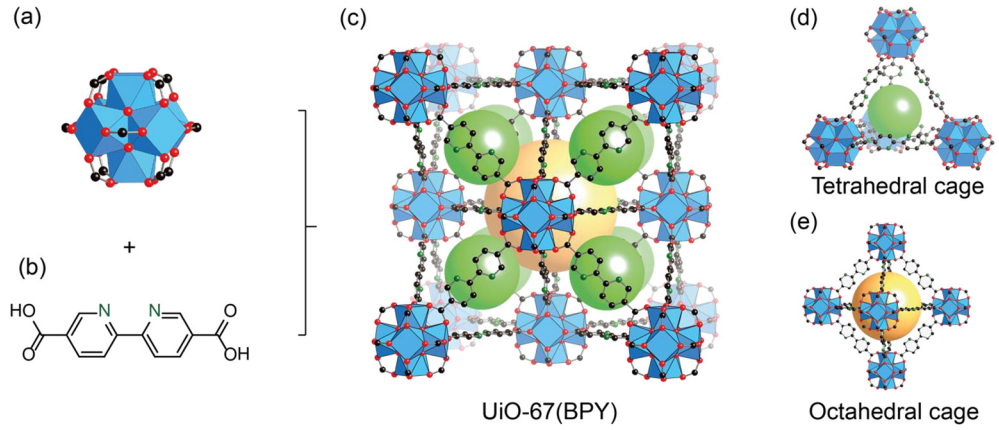

Fig. 2. The $Zr_6(\mu_3\text{-}O)_4(\mu_3\text{-}OH)_4(COO)_{12}$ clusters (a) that are connected by BPY^{2-} linker (b) to form the three-dimensional architecture of UiO-67(BPY) (c). This structure is constructed from a tetrahedral cage (d) and an octahedral cage (e). Atom color: black, C; red, O; green, N; blue, Zr.

the bipyridine docking centers. This has allowed for the systematic alteration of the physical and chemical features of resulting BPY-based Zr-MOFs materials [24,25]. Due to the possibility of one or more types of these specific components, via random deposition, targeted motifs can be anchored or encapsulated within the local heterogeneous environments. These encapsulated or targeted motifs facilitate synergistic interactions between the active components and the host frameworks, thus allowing for the enhancement of properties. However, this has raised an interesting question: can post-synthetic modification be approached and/or advanced via programmed deposition of active encapsulated objects within an ordered framework? In order to gain a deeper understanding, classification of synergistic interactions within MOF frameworks have been divided into several areas: (i) the impact of spreading active centers throughout high porosity MOF platforms; (ii) the comprehensive interactions of similar active centers attached onto the backbone of a MOF structure; (iii) synergistic interactions of bipyridine complexes of different active centers that are positioned near to one another; (iv) interactions between bipyridine complexes attached within the internal surface of Zr-MOFs and those encapsulated within the pores; (v) synergistic interactions of active metal centers at far distances from one another; (vi) interactions among those active centers derived from metal nanoparticles embedded within Zr-MOFs; and (vii) the combined properties of the active complex centers and embedded metal nanoparticles. Throughout literature, we have found distinctly different classifications of these, which result in different outcomes. Hence, there is a need to classify and summarize the entire progress in synthesizing, post-synthetically modifying, characterizing, and applying this important material. Additionally, beyond this, we focus our review on highlighting the applications targeted by BPY-based Zr-MOFs materials.

2. Method for design, synthesis and post-modification of BPY-functionalized Zr-MOFs

UiO-67, an isoreticular structure to the UiO materials (UiO = University of Oslo), was reported for the first time in 2008 and has received considerable attention as a direct result of its crystal structure. UiO-67 is constructed from the highly chemical and thermally stable $Zr_6(\mu_3\text{-}O)_4(\mu_3\text{-}OH)_4(COO)_{12}$ cluster, which is connected together through ditopic biphenyl-4,4′-dicarboxylic acid (H_2BPDC) linkers to yield a three-dimensional face-centered cubic (**fcu**) network. This isostructure is not only attractive because of its topologically beautiful structure, which affords high porosity with 1.6 nm octahedral and 1.2 nm tetrahedral cages, but also from the fact that the BPDC linker can be replaced by 2,2′-bipyridine-5,5′-dicarboxylic acid (H_2BPY). This replacement allows for the design of the UiO-67(BPY) platform with controlled BPY functional groups per each unit cell [24]. Furthermore, BPY-functionalized Zr-MOFs (Fig. 2) and the subsequent incorporation of active components, including metal complexes, nanoparticles and organic functional groups have been synthesized via various synthetic pathways using the specific linkers and active metal centers, as demonstrated in Fig. 3. Herein, we provide a systematic summary of the synthetic strategies for this type of material preparation.

2.1. Method for synthesis of BPY-functionalized Zr-MOFs

The assembly of the H_2BPY linker and the $Zr_6(\mu_3\text{-}O)_4(\mu_3\text{-}OH)_4(COO)_{12}$ cluster, without a modulator, produces UiO-67(BPY) (Fig. 2) with very small particle size [26]. Contrastingly, the direct assembly of these building blocks in the presence of a benzoic acid or acetic acid modulator leads to uniform shape octahedral crystals of UiO-67(BPY) [24,27,28]. Another method that has been employed is the post-synthetic exchange (PSE) method in order to control the incorporation of BPY^{2-} linker into UiO-67. In this synthetic scenario, UiO-67 crystals are immersed in a solution of H_2BPY, under specific conditions, to replace $BPDC^{2-}$ by BPY^{2-}. The amount of BPY^{2-} linker incorporated within the UiO-67 framework can be varied from 0% to 100% and the resulting material retains its high crystallinity and porosity (Fig. 4) [29,30]. Furthermore, the direct assembly of $Zr_6(\mu_3\text{-}O)_4(\mu_3\text{-}OH)_4(COO)_{12}$ clusters in the presence of a mixture of H_2BPY and H_2BPDC linkers represents a convenient method that allows for the design and synthesis of UiO-67(BPY) in a one-step synthesis. This method is termed the "mix-and-match synthetic strategy" (MMS) [31].

2.2. Post-synthetic metalation method (PSM) for the incorporation of active metal complexes in BPY-functionalized Zr-MOFs

Using the obtained UiO-67(BPY), post-synthetic metalation can be considered as a viable method for anchoring active sites of metal complexes onto the backbone of the pristine MOFs to generate the synergistic systems. Specifically, this method was employed by Long et al. who used solution- and gas-phase metalation of UiO-67(BPY) single crystals with different metal precursors ($CuCl_2$, CuCl, $CoCl_2$, $FeBr_2$, and $Cr(CO)_4$) to carry out single crystal-to-single crystal transformation [32]. According to the single crystal X-ray diffraction studies, this resulted in a reduction of

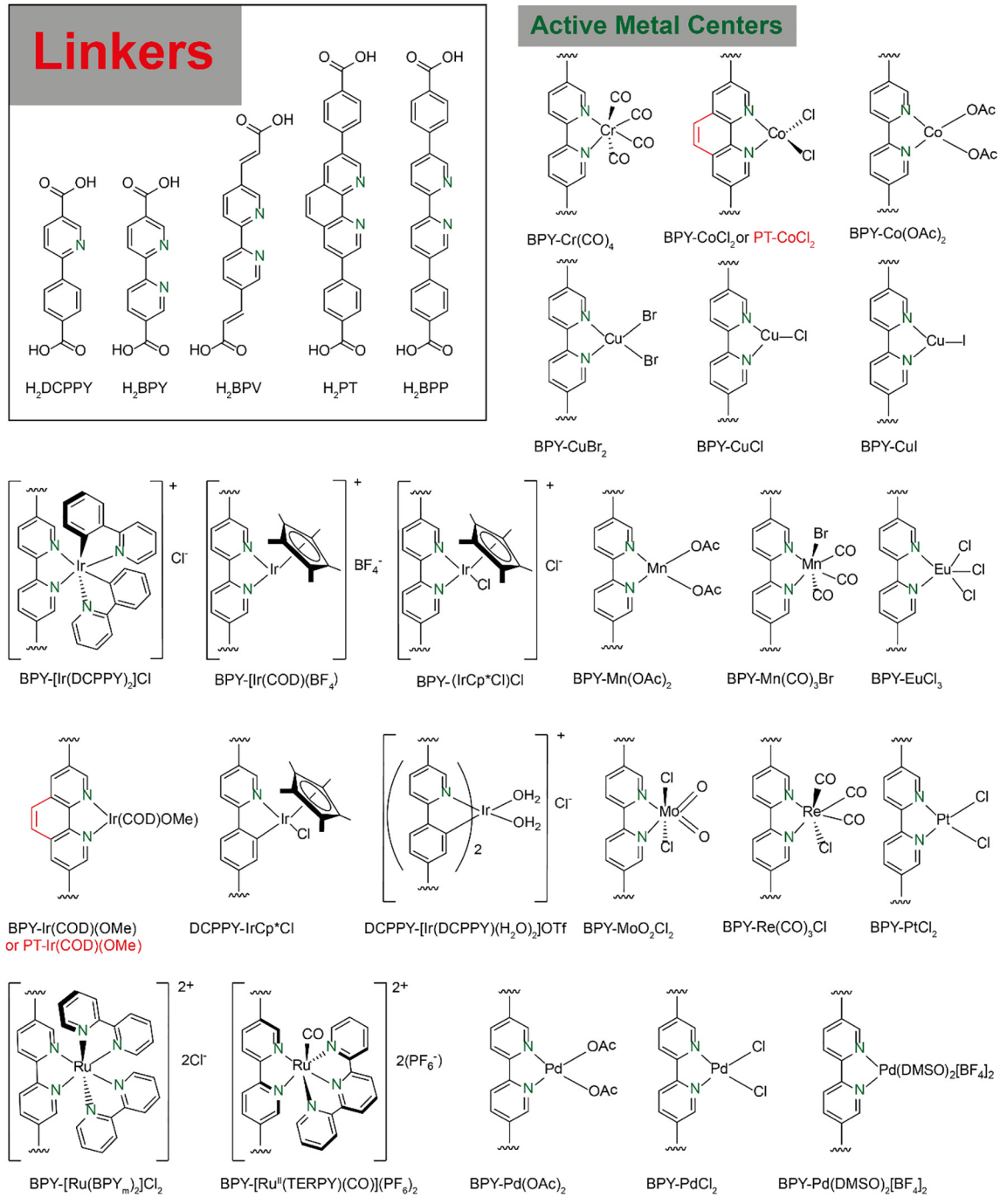

H_2DCPPY = 6-(4-carboxyphenyl)nicotinic acid; **H_2BPY** = [2,2'-bipyridine]-5,5'-dicarboxylic acid; **H_2BPV** = 3,3'-([2,2'-bipyridine]-5,5'-diyl]diacrylic acid; **H_2BPP** = 4,4'-([2,2'-bipyridine]-5,5'-diyl)dibenzoic acid; **H_2PT** = 4,4'-(1,10-phenanthroline-3,8-diyl)dibenzoic acid; **Cp*** = Pentamethylcyclopentadienyl; **COD** = 1,5-Cyclooctadiene; **BPY** = 2,2'-bipyridine functional group; **TERPY** = Terpyridine; **BPY_m** = 2,2'-bipyridine.

Fig. 3. Linkers and active metal center complexes that have been used for the synthesis of BPY-functionalized Zr-MOFs.

structural symmetry for the metalated materials, which was found to be *Pa-3*, a lower symmetry space group when compared to *Fm-3m* of the pristine UiO-67(BPY) (Fig. 5). In an alternative synthetic scenario, organic functional groups, such as methyl halogens, were introduced into UiO-67(BPY) via covalent bonding with the bipyridine groups. This strategy created cationic centers, which later served for targeting applications in anionic attraction [33,34].

2.3. Mix-and-Match synthetic strategy (MMS) for the direct incorporation of BPY functional groups or active metal complexes in BPY-functionalized Zr-MOFs

Despite the successful post-synthetic metalation of BPY-functionalized Zr-MOFs, this method resulted in a high density of active centers inside the structure, which, in turn, led to an overall reduction of the porosity of the materials as well as limited the

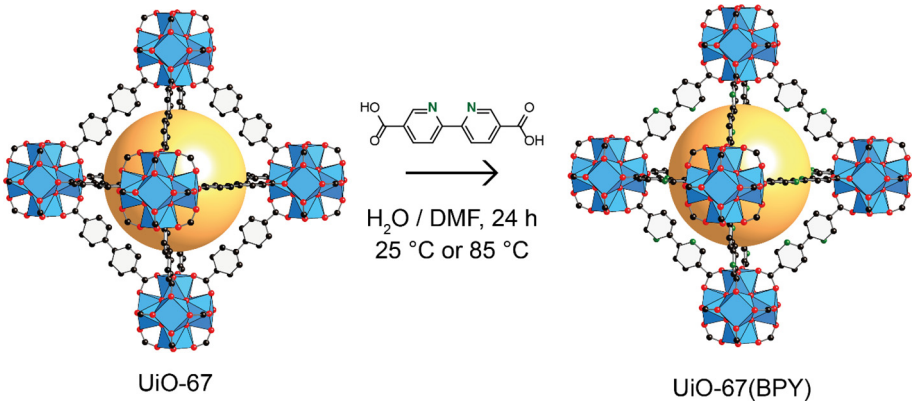

Fig. 4. Post-synthetic linker exchange method towards realizing UiO-67(BPY).

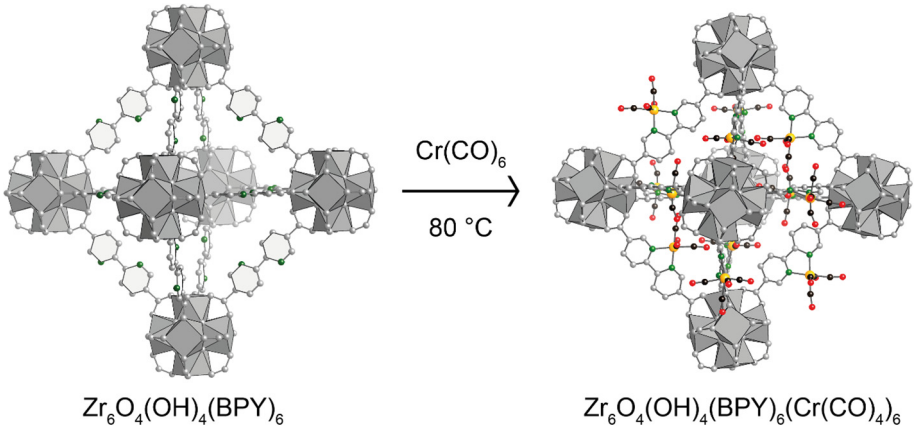

Fig. 5. Post-synthetic metalation via single-crystal-to-single-crystal transformation carried out on the UiO-67(BPY) platform.

effective diffusion of desirable substrates towards the active centers. In this sense, Zr-MOFs with a lower density of BPY functional groups were targeted for post-synthetic metalation. Recently, through the MMS strategy, Manna et al. employed an isoreticular expansion synthetic strategy by using H_2BPV and H_2PT, which led to the development of new BPY-functionalized Zr-MOFs, termed mBPV-MOF and mPT-MOF (Fig. 6). The synthesis of these compounds was carried out in a mixture of Zr metal source together with a mixed linker system (H_2BPHV and H_2BPV for mBPV-MOF; H_2PHN and H_2PT for mPT-MOF, respectively), which allowed for the control of the ratio of BPY incorporation within the resulting Zr-MOFs (Fig. 6). Following this, post-synthetic metalation of these obtained compounds was carried out using an $[Ir(COD)(OMe)]_2$ complex (COD = 1,5-cyclooctadiene). As a result, this combined strategy led to the enhancement in catalytic performance of mBPV-MOF and mPT-MOF as compared to the host BPV-MOF (an isoreticular of mBPV-MOF, which is solely composed of BPV^{2-} linker) [35].

A single step synthesis for the direct incorporation of active metal complexes in Zr-MOFs has also been demonstrated via the MMS strategy. This method employed the utilization of mixed and equal length linkers consisting of complex-decorated BPY-functionalized linkers together with an inactive linker. One of the first examples of this type of MMS was demonstrated by Wang et al., who successfully incorporated the catalytically-active Ir, Re, and Ru complexes of H_2BPY within the framework of UiO-67 (BPY). Interestingly, the reaction of $ZrCl_4$ and pure complex-decorated H_2BPY linker could not produce crystalline materials – the second "inactive" linker was needed. This is presumably due to steric hindrance of these types of complex linkers [31].

Aside from the mixed linker systems, all of which consisted of a single type of active metal center in the Zr-MOF platform, recent progress has been made in the construction of materials with the synergistic combination of Zr-MOF framework with at least two types of active centers. In this case, each type of active center is functional for a half-reaction in a given catalytic cycle. Indeed, this type of system was synthesized via the employment of the MMS strategy by using a mixture of different linkers, typically, H_2BPDC and H_2BPY decorated by various types of active metal centers. Accordingly, several compounds of this sub-class of Zr-MOF materials, such as Ru-Pt@UiO-67 and Pt_n-Ir-UiO-67(BPY) were synthesized and applied for H_2 evolution [36,37]. A one-pot reaction, using mixed metal sources (Ir and Pd or Rh, respectively) in the mixture with H_2BPY and H_2BPDC, was also reported. This combined strategy optimized via various conditions screening leads to the successful synthesis of the metal complex-based UiO-67 (BPY) containing either a controlled amount of iridium metal sites (from 4 to 43 mol%) or dual active metal sites composed of Ir and Pd or Ir and Rh metal complexes [38].

2.4. Method for the incorporation of nanoparticles in BPY-functionalized Zr-MOFs

Furthermore, a strategy towards realizing a synergistic system consisting of mono-/bimetal nanoparticles (NPs) embedded within BPY-functionalized Zr-MOFs have been developed, in which PdNi alloy NPs were encapsulated into MOFs structure by a simple and straightforward assembly of $PdCl_2$ and $Ni(NO_3)_2$ with the reacted solution containing H_2BPY linker and Zr metal source. This

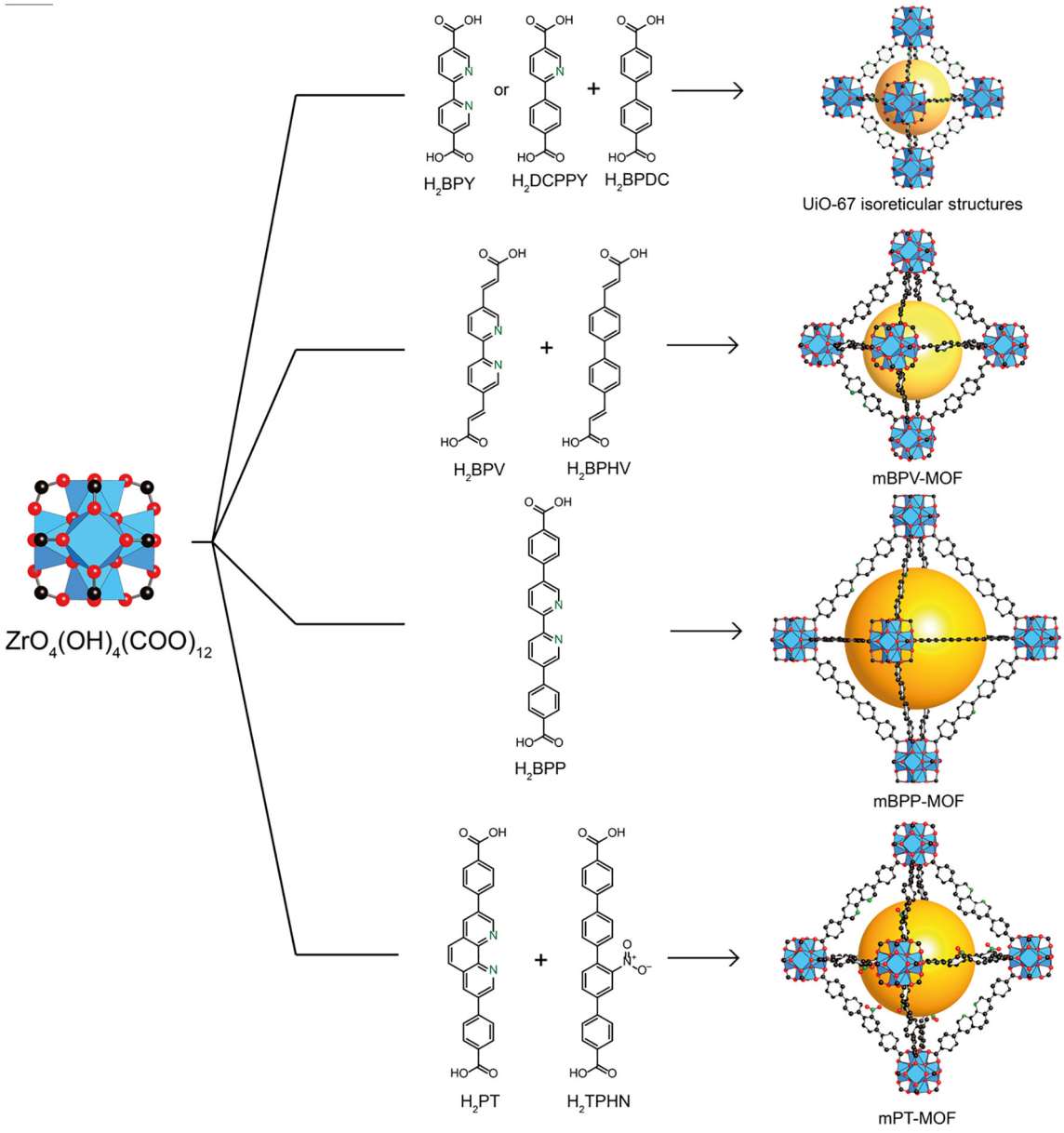

Fig. 6. Employed linkers and their assembly into Zr-based MOFs containing bipyridyl functional groups.

is the so-called *in-situ* incorporation strategy. Following this, the reduction of the BPY complexes-based UiO-67(BPY) was conducted to form the NPs inside the pores of the spongy UiO-67(BPY) material (Fig. 7). This catalytic system was then applied in a hydrogenation reaction, in which the alloy NPs were found to enhance the catalytic properties of the embedded Ni NPs and Pd NPs in Zr-MOFs [39]. Ultrafine bimetallic Pd@Ag core–shell NPs with various Pd/Ag ratios and average sizes of *ca.* 2.6–3.1 nm was also incorporated in the pores of UiO-67(BPY) under a seed-mediated growth strategy using activated hydrogen as the reducing agent. This strategy included multi-step synthesis: (1) Encapsulate Pd NPs within the Zr-MOF through a pre-incorporation method; (2) dissociation and activation of hydrogen molecules on the surface of Pd NPs to serve as effective reducing agents; and (3) selective deposition of Ag on Pd. Indeed, the activated hydrogen atoms, confined on the embedded Pd NP surfaces, promoted the exclusive reduction of Ag^{+} on Pd NPs and prevented significant self-nucleation of Ag to generate individual Ag NPs. This synergistic system consequently exhibited selective enhancement for the hydrogenation reaction [40].

Further advances in this research field led to the flourish of design, synthesis and investigation of the emergent properties, which arose from the interactions between the anchored active complexes and the embedded metal nanoparticles inside the high surface area and large pore volumes of Zr-MOFs. For example, NPs that were wrapped by MOFs have been reported with unusual, but remarkable properties [41]. This methodology modified the environment at the surface of metal nanoparticles, which occurred as a result of the surrounding MOF. Indeed, the synergistic combination of properties, created inside the BPY-functionalized Zr-MOFs, are so far more complicated. Specifically, the surface environment of the wrapped nanoparticles was not only impacted by the surrounding MOFs, but also were modified by the active metal centers attached to the framework backbone. As a result, it is growing interest to produce metal NPs inside the pores of MOFs to obtain highly active and stable heterogeneous catalysts [39]. This type of synergistic system can be synthesized through chemical vapor deposition, liquid/incipient wetness impregnation (solution infiltration), solid grinding, and microwave irradiation [42]. Accordingly, the synergistic hydrogen evolution photo-catalysts, based

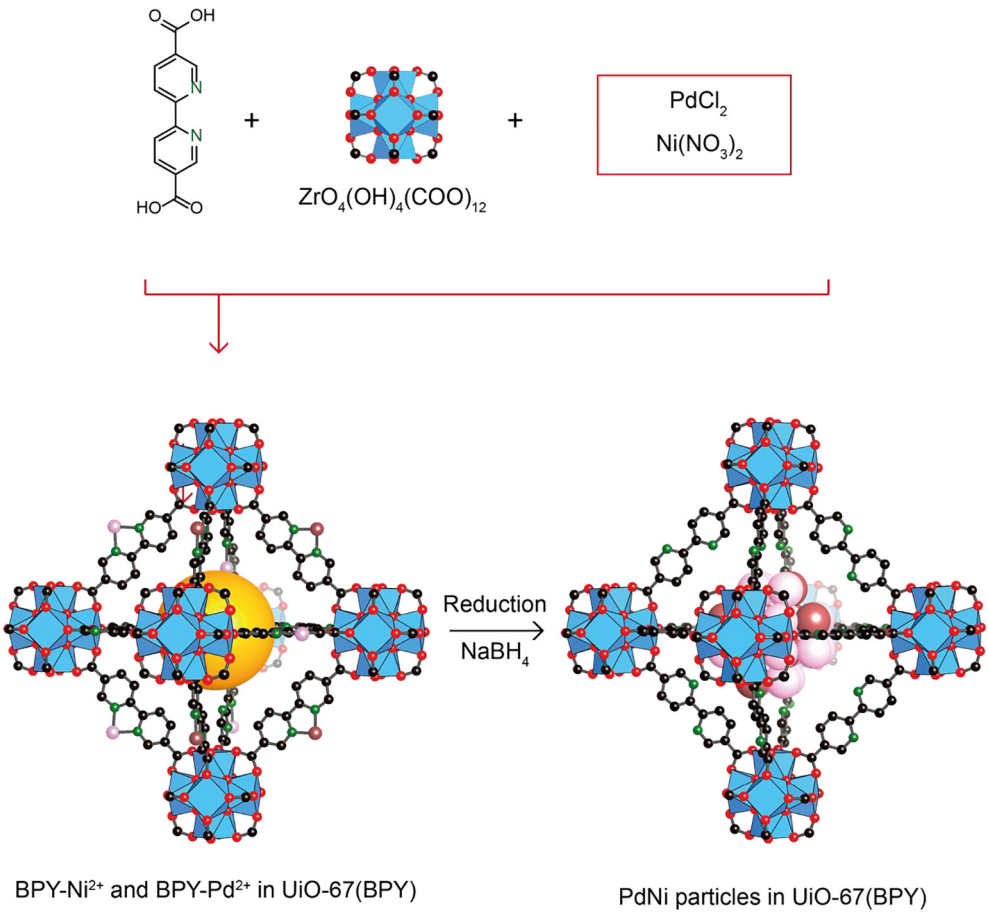

Fig. 7. Synthesis of PdNi alloy NPs inside UiO-67(BPY) via reduction of BPY complex of Ni^{2+} and Pd^{2+}.

on Pt NP@MOF (Pt NP = platinum nanoparticles), were synthesized by Wang et al. via multistep reactions. The authors, initially, employed the MMS to synthesize BPY-functionalized Zr-MOF, which was loaded with BPY-$[Ir(PPY)_2]Cl$ active center. This material was then immersed in a solution containing $KPtCl_4$ and then reduced with TEA under visible irradiation to obtain the final product (Fig. 8). Due to the combined function of different components, this catalytic system was found to be active for H_2 evolution reaction [42].

3. Characterization

Beside well-known analytical methods, such as single-crystal X-ray diffraction (SXRD), new techniques have been utilized to characterize the chemical properties of BPY-functionalized Zr-MOFs, especially to confirm docking agents attached to the backbone or constrained within the pores. Typically, nuclear magnetic resonance spectroscopy (NMR) [29,43] and single-crystal-to-single-crystal transformation were applied as techniques to precisely follow the reaction and to determine the characteristics of the materials [32]. Apart from this, Lamberti et al. used extended X-ray absorption fine structure (EXAFS) and valence-to-core resonant inelastic X-ray scattering (RIXS) techniques to prove the insertion of Pt atoms in the expected framework position of UiO-67(BPY). By using X-ray absorption near edge structure (XANES) spectroscopy, the changes in the Pt oxidation state along with the reaction have been observed, and with EXAFS, the ligand exchange in the first coordination shell of Pt was monitored [44]. In another interesting work, via the combined *in-situ* and operando X-ray absorption spectroscopy (XAS) and Fourier Transform-IR (FT-IR) spectroscopies, Lamberti et al. explored local coordination geometry, redox properties and reactivity of Cu species in the UiO-67(BPY) framework [45]. EXAFS fits and XANES simulations, based on density functionalized theory-optimized geometries, yielded detailed structural and electronic information on the major Cu-species. This was further supported by Hendon et al., who employed the UV-vis-based methodology in combination with computational chemistry and XRD [46]. That methodology has also been applied to characterize a series of Rh-functionalized UiO-67-type catalysts. Recently, Moriss et al. deployed the emission lifetime analysis to investigate the dual occupancy hypothesis at high doping concentrations of $Ru(BPY)_2Cl_2$ in UiO-67(BPY). This was used to confirm whether the complex can be incorporated into the framework backbone of UiO-67(BPY) or, alternatively, was encapsulated in the pores [47,48]. According to the authors, a hypothesis was proposed, for which, if the monophasic 1.4 μs emission lifetime decay was observed at low doping concentrations, this would be attributed to BPY-$[Ru(BPY_m)_2]Cl_2$ incorporated into the backbone of UiO-67(BPY). On the other hand, if a bi-exponential expression with slow and fast lifetime components was observed at higher doping concentrations, which are on the order of 200 ns and 20 ns, it would be attributed to dual occupancy, in which, the fast lifetime component was assigned to a non-incorporation of $Ru(BPY)_2Cl_2$ encapsulated in UiO-67(BPY) pores and the low lifetime component was ascribed to those incorporated into the UiO-67 backbone [47]. This hypothesis was further confirmed by various model fitting based on emission lifetime analysis [47] with confocal fluorescence microscopy employed parallel to probe for the distribution of BPY-$[Ru(BPY_m)_2]Cl_2$ and $Ru(BPY)_2Cl_2$ throughout the whole crystal of UiO-67(BPY) [48].

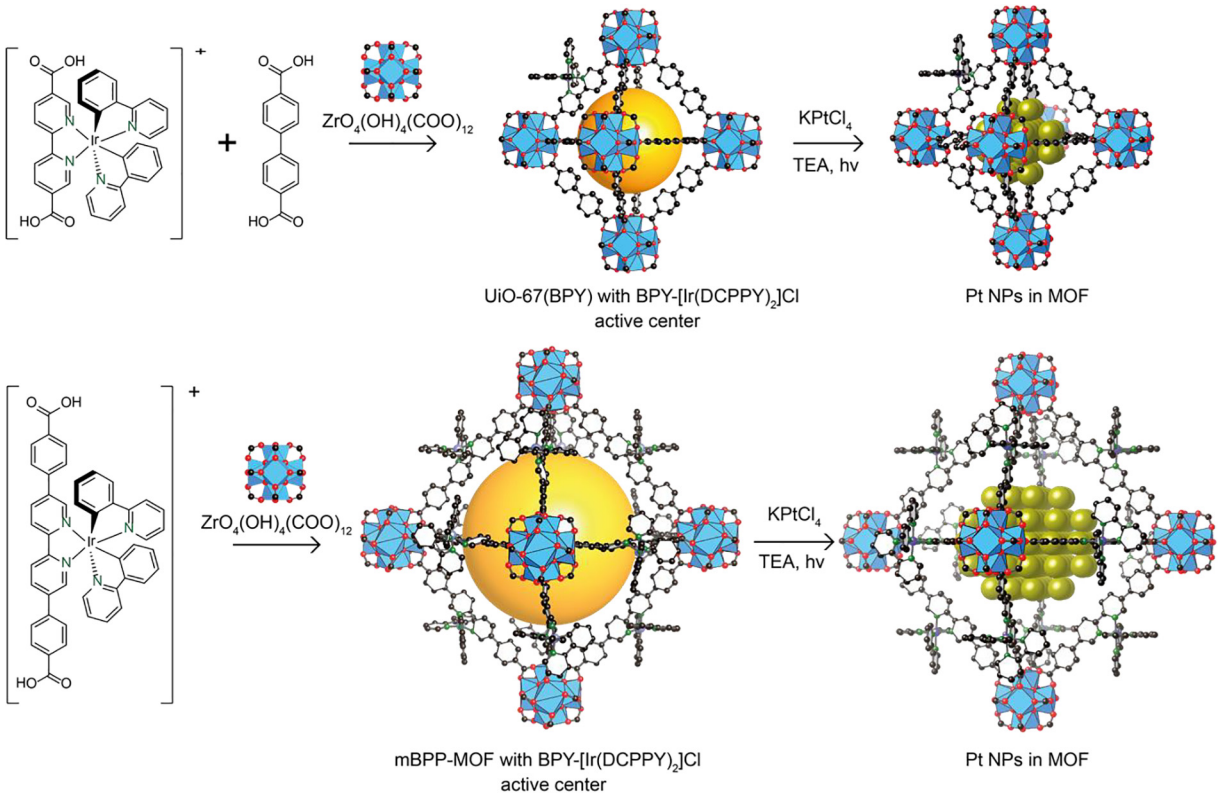

Fig. 8. Synthesis of phosphorescent Zr-MOFs of the **fcu** topology with loading of Pt NPs inside the MOF cavities. This occurs via MOF-mediated photoreduction of K_2PtCl_4 to form the Pt NPs.

4. Applications

Indeed, the flexibility in design and synthesis as well as the viable pathways to dock active metal centers via the 2,2′-bipyridyl functional group, granted the BPY-functionalized Zr-MOF platform the unique opportunity to combine the interesting properties of particular complexes within one porous platform, in which these active components can then interact with one another to produce the synergistic combination of properties, which cannot otherwise be observed by the homogeneous complex alone. In this section, we discuss the applications of BPY-functionalized Zr-MOFs, which range from catalysis, molecular adsorption, luminescence sensing, and other applications applied to clean energy. It is noted that we not only summarize the novel applications achieved as a result of the designed materials, but detail a viewpoint that focuses on how these properties arise from a synergistic combination of constituent components.

4.1. Catalysis

Catalysis is an important application of MOFs, which can be performed via two strategies: (i) deploying catalytic active centers, which exist naturally in the metal clusters or linkers; or (ii) immobilizing active centers onto the internal surface of MOFs via coordinated or covalent bonds. An ever-increasing number of reports and comprehensive reviews have been reported for this research field [49–53]. As discussed through the review, the applications based on BPY-functionalized Zr-MOFs with designed active centers, play a crucial role in MOFs research. In brief, it is worth noticing that the synergistic combination of emerging properties such as the high surface area of Zr-MOFs and the active centers constrained within the pores, contributed significantly to improve catalytic stability, which, in turn, has afforded higher catalytic performance. Additionally, there are tendencies in the synthesis and applications of Zr-MOFs with the multi-type active centers or nanoparticles to create combined interactions between the active components in order to fulfill the mechanism of specific catalytic reactions. On the contrary, several catalysts possessing constrained active centers exhibited lower turnover frequency than their homogeneous analogues as the platform prevented contact by the active agents with substrate molecules. Thus, additional approaches to overcome these posed challenges are required. Herein, we provide a systematic review on the catalytic applications of BPY-functionalized Zr-MOFs for CO_2 reduction, hydrogen evolution and oxidation in the context of the synergistic interaction between the catalytic components and the framework. The summary for the applications of these materials in catalysis has been specifically provided in Table 1.

4.1.1. Photocatalysis for CO_2 reduction

CO_2 reduction represents the most focused research, aiming to reduce emitted CO_2 in the Earth's atmosphere and turn this gas into fuels and chemical feedstock. CO_2 reduction not only helps to balance atmospheric CO_2 levels and its consequential global warming effects but also generates the sustainable energy source. Traditional catalysts for CO_2 reduction invoke the utilization of homogeneous rhenium complexes, however, this catalyst suffers from the fast decomposition due to dimerization and leads to an overall reduction in the catalytic activity. In this sense, Zr-MOFs coupled with metal complexes of BPY have received considerable attention as efficient catalysts for CO_2 reduction. Indeed, several catalytic active metal sites were immobilized in Zr-MOFs, for example: BPY-[$Re^{I}(CO)_3Cl$]; BPY-[Ru^{II}-(TERPY)(CO)]$(PF_6)_2$ and BPY-$Mn(CO_3)Br$. As a result, the catalytic stability of Zr-MOFs, decorated with the active complexes were enhanced in comparison with homogenous BPY-[$ReI(CO)_3Cl$] catalyst, which normally suffered from fast decomposition. The higher accumulated TONs for CO_2 reduction was observed when

Table 1
Applications of functionalized UiO-67(BPY) in catalysis.

No.	Material	Active Centers	Applications	Result	Refs.
MOFs for CO_2 Reduction					
1	Ag⊂Re_n-MOF	BPY-$Re(CO)_3Cl$ and Ag nanoparticles	Reduction of CO_2 to CO	7-Fold enhancement of CO_2-to-CO conversion under visible light (in comparison with Re_3-MOF), stability at least 48 h	[56]
2	MOF 4	BPY-$Re(CO)_3Cl$		TON = 10.9, after 20 h	[31]
3	Zr-BPDC/ RuCO	BPY-[Ru^{II}(TERPY)(CO)]$(PF_6)_2$		TON = 9, after 6 h	[54]
4	UiO-67-Mn(BPY)$(CO)_3Br$	BPY-$Mn(CO)_3Br$	Reduction of CO_2 to formate	TON ~ 110, after 18 h	[55]
MOFs for Hydrogen Evolution					
5	Zr-MOF-BPY-$PtCl_2$	BPY-$PtCl_2$	Photocatalyst for hydrogen production reaction from water	Hydrogen evolution of 8.3 μmol after 9 h which is higher than (BPY)$PtCl_2$ complex.	[57]
6	Pt@1 [Pt NP@MOF] Pt@2 [Pt NP@MOF]	BPY-[$Ir(DCPPY)_2$]Cl and Pt nanoparticles BPP-[$Ir(DCPPY)_2$]Cl and Pt nanoparticles	Photocatalyst for hydrogen evolution by synergistic photoexcitation	With higher turnover numbers (1.5 and 4.7 times) than those of the homogeneous controls.	[42]
7	Pt@UiO-67 Ru-Pt@UiO-67	BPY-$PtCl_2$ [BPY-$Ru(BPY)_2$]Cl_2-$PtCl_2$	Photosensitizer and catalyst hydrogen generation from water	Ru-Pt@UiO-67 has a high activity with a generation of 0.5 μmol H_2 after 5 h irradiation at pH = 5.	[36]
8	Pt_n_Ir_BUiO	BPY-[$Ir(DCPPY)_2$]Cl-$PtCl_2$	H_2-evolving catalyst and photosensitizer	Enhance stability and no colloidal formation for at least 6.5 days, the molecular catalyst becomes colloid just after 7.5 h.	[37]
MOFs for C–H Borylation					
9	UiO.[Ir(COD)$(BF_4)]_{0.6}$	BPY-Ir(COD)(BF_4)	Catalyst for Benzene C–H Borylation with B_2pin_2	**Yield**: 94%, 80 °C, 24 h	[32]
10	BPV-MOF-Ir mBPV-MOF-Ir mPT-MOF-Ir	BPV-[Ir(COD)$(OMe)]_2$ mBPV-[Ir(COD)$(OMe)]_2$ mPT-[IrCl(COD)$]_2$	Arene C–H borylation	**Yield**: 100% with mBPV-MOF-Ir and mPT-MOF-Ir	[35]
11	BPY-UiO-Ir	BPY-Ir(COD)(OMe)	Catalyst for Borylation of aromatic C–H bonds	**Yield**: 83–95%	[58]
12	mPT-MOF-$CoCl_2$	PT-$CoCl_2$	Arene C–H borylation	**Yield**: 100% for almost all substrates.	[59]
MOFs for Oxidation					
13	MOF 1	DCPPY-IrCp * Cl	Catalyst for water oxidation	TOF = 4.8 h^{-1}	[31]
14	MOF 2	BPY-(IrCp * Cl)Cl		TOF = 1.9 h^{-1}	
15	MOF 3	DCPPY-[Ir(DCPPY)$(H_2O)_2$]OTf		TOF = 0.4 h^{-1}	
16	UiO-67-MoO_2Cl_2(BPY)	BPY-MoO_2Cl_2	Catalyst for the epoxidation of cis-cyclooctene and limonene	**Selectivity/conversion (%):** 100%/97% for cis-cyclooctene and 90%/67% for limonene at 75 °C.	[60]
17	UiO-67(BPY)-$CuBr_2$	BPY-$CuBr_2$	Catalyst for the selective oxidation of cyclooctene to cyclooctene oxide	**Yield/conversion(%):** 84.3/95.3% after 12 h.	[61]
18	MOF-53 MOF-53-VCl_3 MOF-53-VCl_4	BPDC and BPY	Coupling of epichlorohydrin with carbon dioxide	**Yield**: 79.6% for MOF-53 (highest yield among three samples).	[62]
MOFs for Catalyst with Palladium Active Center					
19	BPY-MOF-$PdCl_2$ m-4,4′-Me_2BPY-MOF-$PdCl_2$ m-6,6′-Me_2BPY-MOF-$PdCl_2$	BPY-$PdCl_2$	Catalyst for Suzuki-Miyaura cross-coupling reaction	**Highest yield**: 90%, m-6,6′-Me_2BPY-MOF-$PdCl_2$ catalyst	[43]
20	UiO-67(BPY)-Pd	[$Pd(CH_3CN)_4$][BF_4]$_2$	Dehydrogenation of cyclohexenones to phenol	**Highest yield:** 93%, using DMSO at 100 °C.	[58]
21	BPY-UiO-Pd$(OAc)_2$	BPY-$Pd(OAc)_2$	Catalyst for the reaction of phenylboronic acid with 3-methylcyclohex-2-en-1-one	**Highest yield:** 99%, catalyst containing 8.1 wt% Pd.	[63]
22	Pd(II) doped UiO-67	BPY-$PdCl_2$	Catalyst for Heck coupling and Suzuki-Miyaura reaction	**Yield**: 80–99%	[64]
MOFs for other Transformations					
23	MOF 5	BPY-[$Ir(DCPPY)_2$]Cl	Photocatalyst for aza-Henry reaction	**Highest conversion:** MOF 5: 96% MOF 6: 97%	[31]
24	MOF 6	[BPY-$Ru(BPY)_2$]Cl_2	Photocatalytic aerobic amine coupling reaction Photo-oxidation of thioanisole	**Highest yield:** MOF 6: 90% **Conversion**: MOF 6: 76%, after 22 h	
25	BPV-MOF-Ir mBPV-MOF-Ir mPT-MOF-Ir	BPV-[Ir(COD)$(OMe)]_2$ mBPV-[Ir(COD)$(OMe)]_2$ mPT-[IrCl(COD)$]_2$	Hydrosilylation of aryl ketones and aldehydes by dehydrogenative ortho-silylation of benzylicsilyl ethers.	100% yield with most of the used catalysts.	[35]

(*continued on next page*)

Table 1 (*continued*)

No.	Material	Active Centers	Applications	Result	Refs.
26	BPY-MOF-$CoCl_2$ BPV-MOF-$CoCl_2$ mBPP-MOF-$CoCl_2$	BPY-$CoCl_2$ BYV-$CoCl_2$ BPP-$CoCl_2$	Alkene hydrogenation, hydroboration and aldehyde/ketone hydroboration	-TON of up to 2.5×10^6 and turnover frequencies (TOFs) of up to $1.1 \times 10^5 h^{-1}$ for alkene hydrogenation. -Hydroboration of alkene: The highest yield with mPT-MOF-$CoCl_2$ is 100% for each substrate. -Hydroboration of ketone and aldehyde: Using BPV-MOF-$CoCl_2$ (0.05 mol% Co) with a yield of 100%.	[59]
27	UiO-67-Ru$(BPY)_3$	[Ru$(BPY)_2(H_2DCBPY)$]	Catalyst for the aerobic oxidative hydroxylation of arylboronic acid	**Highest yield:** 81% for UiO-67-[Ru$(BPY)_3]_{0.1}$	[65]
28	UiO-67-Co$(BPY)_{0.25}$ UiO-67-Mn$(BPY)_{0.25}$	BPY-$Co(OAc)_2$ BPY-$Mn(OAc)_2$	Micromotors in fuel solutions	Designing micromotor with a high degree of motion and a chemical "braking" system.	[66]
29	PdNi-in-UiO-67	BPY-$PdCl_2$/$NiCl_2$	Catalyst for the hydrogenation of nitrobenzene to aniline	Yield: 100% after 3 h, 25 °C.	[39]
30	Pd@Ag-in-UiO-67	BPY-$PdCl_2$ and Ag nanoparticles	Catalyst for hydrogenation of phenylacetylene to styrene	Selectivity (91%) as compared to monometallic Pd NPs confined in UiO-67 (75% selectivity).	[40]

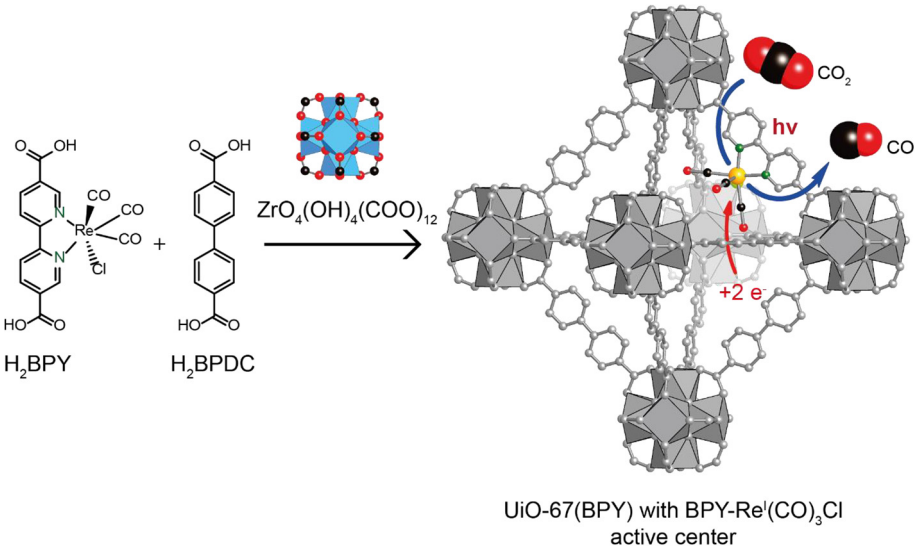

Fig. 9. CO_2 reduction to CO via photocatalyst at BPY-$Re^I(CO)_3Cl$ active center.

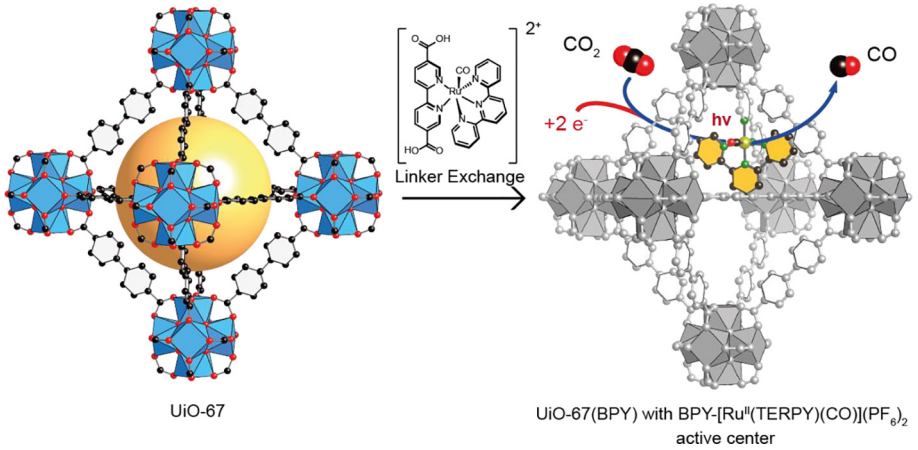

Fig. 10. CO_2 reduction to CO via photocatalyst at BPY-[Ru^{II}(TERPY)(CO)]$(PF_6)_2$ active center.

using post-synthetically modified MOF catalysts compared with the homogeneous complexes.

Accordingly, Wang et al. reported the method to synthesize ($Zr_6(\mu_3\text{-}O)_4(\mu_3\text{-}OH)_4(BPDC)_{6-x}(\mathbf{L})_x$) (L = H_2BPY with the respective active metal complexes) by MMS, in which, the active linker (H_2BPY-[$Re^I(CO)_3Cl$]) was designed to match the length of H_2BPDC linker. This led to the anchoring of BPY-[$Re^I(CO)_3Cl$] onto the internal surface of UiO-67(BPY) [31] resulting in the combination of

properties between BPY-[$Re^{I}(CO)_3Cl$] active complex and the high surface area of MOFs arose, as the platform virtually provided the anchored points to prevent the self-dimerization and supported fast diffusion of electron sacrificial donors (triethylamine). This catalyst further exhibited high activity for photocatalytic CO_2 reduction, as proven by three-time enhancement of a total turnover number (TON) of 10.9 times after 20 h (Fig. 9) compared to its homogeneous complex performance.

Similarly, BPY-[Ru^{II}(TERPY)(CO)]$(PF_6)_2$ active center was introduced in UiO-67 via PSE of metalloligand. This compound, termed MOF-Ru^{II}-composite, was constructed from both $BPDC^{2-}$ and BPY^{2-} linker, which post-synthetically bore BPY-[Ru^{II}(TERPY)(CO)]$(PF_6)_2$ active center causing the dispersion of BPY-[RuII(TERPY)(CO)]$(PF_6)_2$ active complex onto the surface of UiO-67 (BPY). MOF-Ru^{II}-composite was then used for CO_2 reduction under visible light to produce CO, HCOOH, and H_2. The TONs for CO_2 reduction to CO was found to be 9 times after 6 h reaction (Fig. 10). The MOF-Ru^{II}-composite exhibited high catalytic activity, even at low CO_2 concentrations. Furthermore, the catalytic activity of this composite was comparable with the corresponding homogeneous Ru^{II} catalyst and ranked among the highest performing known MOF-based catalysts used for CO_2 reduction conducted under photocatalytic conditions [54].

Moreover, the combined interactions of multi-active centers, dispersed throughout the internal surface of MOFs, have been adopted to design synergistic systems for CO_2 reduction. Specifically, Mn(I) active metal complexes have been docked into the structure of UiO-67(BPY) to serve as the catalytic active centers, which interacted directly with CO_2 to reduce this substrate. This complex, however, can only properly function with the flux of electrons from the interaction with a $[Ru(DMB)_2]^{2+}$ photosensitizer (DMB = 4,4′-dimethyl-2,2′-bipyridine). Finally, this synergistic system was fulfilled through the employment of electron sacrificial donor agents (triethanolamine, TEA), which via the oxidized process at $[Ru(DMB)_2]^{2+}$ photo-sensitizer, allowed the supply of desired electrons into the catalytic cycle. As a result, this composite was found to be effective for catalysing CO_2 reduction to generate formate product with maximum TONs of 110 times after 18 h reaction. Interestingly, this catalyst could be reused several consecutive cycles and the increased activity of the Mn-containing MOF was attributed to the isolated active sites, which prevent dimerization of the Mn complex [55]. An artificial photocatalyst, designed with the collaborative interactions between the nanoparticles and active metal complexes, was then synthesized. The construction of this system was focused on the synthesis of an Ag nanoparticle core, which was wrapped by BPY-functionalized Zr-MOFs, decorated with BPY-$Re^{I}(CO)_3Cl$ active sites. This system was termed Ag⊂Re_n-MOF (n = 0, 1, 2, 3, 5, 11, 16, and 24 complexes per unit cell). The experimental analysis indicated that Ag⊂Re_3-MOF (MOF layer, 16 nm) exhibited 7-fold enhancement of CO_2-to-CO conversion under visible light over the Re_3-MOF. This, indeed, was attributed to spatial confinement of photoactive Re centers covering the plasmonic fields at the surface of Ag nanocubes. The long-term stability of the composites was found for at least 48 h, which suggested the long-term working stability of this composite. On the other hand, in terms of catalytic performance of Ag⊂Re_3-MOF, the initial TON for the first several hours was far less than BPY-$Re^{I}(CO)_3Cl$ homogenous catalyst, thus further improvement is needed to synthesize better catalysts [56].

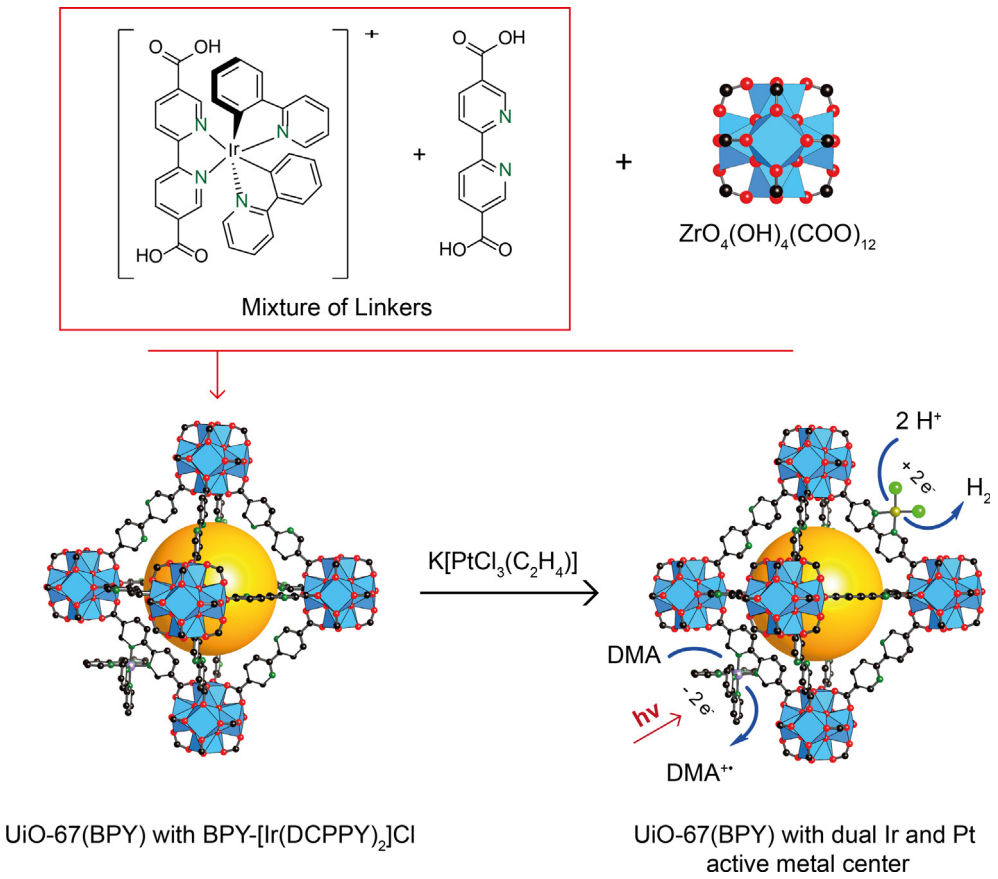

Fig. 11. Synthesis of the dual sites active metal center of Ir-Pt@UIO-67(BPY) and its photocatalytic mechanism.

4.1.2. Hydrogen evolution

Hydrogen fuel represents a clean and sustainable energy source, which has the potential to play an important role in the replacement of depleting fossil fuels. With respect to the evolution of hydrogen, it is essential to design a system that can catalyze two half-reactions, the H^+ reduction and water oxidation. Indeed, the design of such systems in one catalyst is obviously very challenging. However, it is noted that current efforts have paved the way towards the design and synthesis of catalysts for separate H^+ reduction and water oxidation, with the perspective of combining both catalysts within one catalytic system. For H^+ reduction, two different approaches have been considered. In the first method, catalysis is driven by electricity to evolve hydrogen and in the second method, catalysis is driven by solar energy. For hydrogen evolution driven by solar energy, a complex reaction system must be developed, which includes the combination of light harvesting elements, sacrificial electron donors, electron mediators, and hydrogen-evolving catalysts. Hence, the synergistic combination of properties of active catalysis centers is required to perform such challenging reactions. Indeed, recent efforts are aimed at enhancing the reaction yield, solar energy efficiency, and stability of the reaction system through sophisticated design, in which each active center plays a different role and interacts with each other to assist the reactions.

Toyao et al. prepared UiO-67(BPY) loaded $PtCl_2$ for photocatalytic hydrogen production under visible-light irradiation ($\lambda > 420$ nm) in water containing TEA, which acted as the sacrificial electron donor. The prepared catalyst achieved steady hydrogen evolution with the amount of evolved hydrogen reaching 8.3 μmol after 9 h, which was higher than the corresponding homogeneous BPY-$PtCl_2$ complex [57]. Moreover, the photo-electron system, composed of dual active metal centers, included the photosensitizer BPY-$[Ru(BPY_m)_2]^{2+}$ and the proton reduction catalyst BPY-$PtCl_2$, was successfully incorporated into the backbone of UiO-67 (BPY), via the MMS strategy [36]. This bi-metallic Ru-Pt@UiO-67 (BPY) material exhibited an enhancement in hydrogen evolution in aqueous solution at pH 5.0 under visible light irradiation. It is stated that "this Ru-Pt@UIO-67 system represents the first example of MOFs functionalized with two different transition metal complexes", which respectively acted as the photosensitizer and catalyzed for hydrogen evolution from water [36]. Similarly, Kim et al. prepared a self-healing system, which "spontaneously repaired [the] molecular catalyst and photosensitizer" during photocatalytic H_2 evolution. Accordingly, an Ir complex was immobilized onto the surface of UiO-67(BPY) by MMS strategy, following by post-metalation with $K[PtCl_3(C_2H_4)]$ to form Pt_n-Ir-UiO-67 (BPY). This synergistic system was then used as photocatalyst for H_2-evolution (Fig. 11). Indeed, the $Pt_{0.1}$-Ir-UiO-67(BPY) catalyst exhibited very stable molecular photocatalysis without any significant decrease in catalytic activity nor colloidal formation for at least 6.5 days. This outperformed the homogeneous molecular catalyst, which became a colloid after just 7.5 h. The stability was explained by efficient self-healing caused by the arrangement of diamine sites that closely and densely surrounded the H_2-evolving catalyst and photosensitizer sites in the Zr-MOF [37].

Synergistic hydrogen evolution photocatalysts based on Pt NP@MOF were reported by Wang et al., who successfully loaded Pt NPs into the pores of phosphorescent BPY-functionalized Zr-MOF, which was decorated with BPY-$[Ir(PPY)_2]Cl$ active center. This synergistic compound was found to efficiently photocatalyze H_2 evolution under visible light (>420 nm). In detail, the BPY$^{\cdot-}$-$[Ir^{III}(PPY)_2]$ radicals were generated under visible light illumination via the interaction with TEA promoting the electrons transfer from the active metal complexes into Pt NPs (*i.e.* Photoinjection of electrons). Furthermore, this catalyst was found to have higher turnover frequencies and turnover numbers (1.5 and 4.7 times) than those of the homogeneous catalysts, explained by a facile electron transfer, not otherwise observed in homogeneous catalysts, from the photo-reduced Ir phosphor to the entrapped Pt NPs inside the MOF catalytic system [42].

4.1.3. Catalysis for C−H borylation

C−H borylation represents an important reaction to transform inert chemical feedstock into valuable fine chemicals. Traditional catalysts promoted for C−H borylation, were deployed iridium complexes with N-donor ligands, which consequently face the challenge of high cost-effectiveness and non-sustainability for large-scale reactions. Indeed, immobilizing of iridium complexes on a porous platform not only allow the catalyst to be recycled but also do not cause any loss of catalytic properties from the active iridium centers [32]. Additionally, a higher level of synergistic combination of properties of this type of materials can be synthesized and applied for the cascade reactions via the synthesis of the synergistic catalyst consisting of dual active metal centers of Ir and Pd-functionalized Zr-MOFs. This catalyst, in perspective, can proceed C−H borylation as well as C–C bond formation to target the final product within one step reaction.

Recently, UiO-67(BPY) was employed as a solid platform for docking of iridium complex via post-synthetic metalation strategy. This further generated BPY-Ir(COD)(OMe) active center on UiO-67 (BPY) platform, termed UiO-67(BPY)-Ir. The resulting catalytic reaction indicated that the Ir-functionalized Zr-MOF exhibited high catalytic activity for borylation of aromatic C−H bonds with $B_2(pin)_2$ (pin = pinacolate). Furthermore, this catalyst can be reused up to 20 times for the borylation without any loss of catalytic activity or crystallinity [58]. Similarly, the new heterogeneous catalyst has been synthesized via post-synthetic metalation by docking of $[Ir(COD)_2]BF_4$ onto the surface of UiO-67(BPY). This consequently resulted in the BPY-[Ir(COD)] (BF_4)-functionalized UiO-67(BPY) platform acted as a heterogeneous catalyst for the C−H borylation of benzene to form 4,4,5,5-tetramethyl-2-phenyl-1,3,2-dioxaborolane with a yield of 100% at very low catalyst loading (Table 1) [32]. Taking advantage of the catalytic performance of this material, an isoreticular version of UiO-67 was expanded, termed mBPV- and mPT-MOF, which contained bipyridyl- and phenanthryl-based linkers and linkers without chelating groups (Fig. 6). The post-synthetic metalation of these MOFs with $[Ir(COD)(OMe)]_2$ generated BPV-Ir(COD) (OMe) and PT-Ir(COD)(OMe) functionalized Zr-MOFs, respectively. This Ir-functionalized MOFs exhibited high catalytic performance for C−H borylation of arenes using B_2pin_2 with mostly 100% yield [35]. As an effort towards low cost and sustainable technology, an earth-abundant metal (Co) was considered as a replacement to the iridium complexes for the catalysis of alkene hydroboration, aldehyde/ketone hydroboration, and arene C−H borylation. These catalysts were synthesized via immobilization of $CoCl_2$ on UiO-67 (BPY), BPV-, mBPP- and mPT-MOF to produce BPV-$CoCl_2$, BPP-$CoCl_2$ and PT-$CoCl_2$ active centers, respectively. The resulting heterogeneous catalysts displayed turnover numbers (TONs) up to 22.0×10^3, 48.0×10^3 and 1.0×10^3 times for alkene hydroboration, aldehyde/ketone hydroboration and C−H borylation of arenes, respectively [59].

4.1.4. Oxidation

It is desirable to develop the new heterogeneous catalysts to achieve high yield and selectivity in oxidation reactions. In this regard, controlling the conditions as well as designing the catalysts in oxidation reactions to achieve the desired products and prevent those products from further oxidized processes (reaction termination) is important. Indeed, UiO-67(BPY) platforms with selected active metal centers have also been employed for this specific application. Accordingly, the BPY-functionalized UiO-67,

consisting of iridium complexes, was synthesized by the MMS strategy. This kind of catalyst was found to be active for water oxidation with turnover frequencies (TOFs) up to 4.8 h^{-1} [30]. In another report, the reaction between H_2BPDC, H_2BPY-(MoO_2Cl_2) complex, and $ZrCl_4$ generated the UiO-67(BPY) catalytic platform incorporating BPY-MoO_2Cl_2 active centers. Subsequently, this catalyst, termed UiO-67-MoO_2Cl_2(BPY), was found to be useful for the epoxidation of *cis*-cyclooctene and limonene in the presence of *tert*-butylhydroperoxide and trifluorotoluene at 75 °C, which acted as an oxidant and co-solvent, respectively. This resulted in epoxide selectivities of 100% for *cis*-cyclooctene with 97% conversion, and 90% for limonene with 67% conversion [60]. Similarly, immobilization of $CuBr_2$ onto the internal surface of UiO-67(BPY) generated BPY-$CuBr_2$-functionalized UiO-67(BPY) whose structure possessed an immobilized square planar Cu complex as proven by XAFS and UV−vis spectroscopy. The epoxidation of cyclooctene in the presence of *tert*-butyl hydroperoxide was promoted by this catalyst with high catalytic activity as demonstrated by 84.3% yield and 95.3% selectivity. On the other hand, a significantly lower yield of that reaction was found when using the homogeneous complex of BPY-$CuBr_2$ catalyst. As such, this indicated that the cooperative interaction between the active metal centers and the surrounding environment provided by MOFs enhanced the yield and selectivity for this oxidation reaction [61].

Demir et al. prepared $Zr_6O_4(OH)_4(HCOO)_2(BPDC)_2(BPY)_3$ (MOF-53) using the MMS strategy with formic acid as the modulator (Fig. 12). MOF-53 was subsequently used as the platform for anchoring of vanadium active centers via post-synthetic metalation with VCl_3 and VCl_4 to obtain MOF-53-VCl_3, and MOF-53-VCl_4, respectively. These composites were demonstrated active for the coupling reaction of epichlorohydrin with carbon dioxide. Interestingly, pure MOF-53 exhibited higher catalytic activity (yield: 96.4%; selectivity: 97.4%; TON and TOF values were 964 and 482, respectively) than UiO-67 and UiO-67(BPY) while MOF-53-VCl_3, and MOF-53-VCl_4 exhibited no positive effect on the yield because of the lower surface area and pore volume of the later materials [62].

4.1.5. Catalysis on UiO-67(BPY) with palladium active center

Palladium complexes are known to be effective catalysts for a wide range of important reactions in laboratory as well as large-scale industrial system. However, the homogenous nature of the Pd complexes prevents them from effective recycling, thus, it raises the cost for using this catalyst in large-scale organic synthesis. Another consideration for using this type of catalyst is the decomposition of the complex with the aggregation of Pd during the reactions contaminated the products. With all of this taken in account, it raises the demand to design the highly active heterogeneous Pd catalyst, which are stable and reusable. Indeed, immobilization of Pd complexed onto the internal surface of MOFs has emerged as a viable approach, in which the Pd complex is distributed onto the surface of MOFs via strong interactions through secure docking centers to prevent aggregation and allow the catalysts to be recycled. Accordingly, the composite material of UiO-67(BPY), doped with BPY-Pd$(DMSO)_2[BF_4]_2$, was found to effectively catalyze the dehydrogenation of various substituent-derived cyclohexenones, in the presence of oxygen, which acted as the oxidant at ambient pressure, to produce phenol derivatives. This material also afforded high catalytic activity for dehydrogenation in DMSO at 100 °C with the maximum yield up to 93% [58]. Interestingly, significant enhancement in the catalytic activity has been observed for Suzuki-Miyaura cross-coupling reactions by using UiO-67(BPY-Me_2) catalyst docked with Pd(II) [where BPY-Me_2 = 6,6′-dimethyl-(2,2′-bipyridine)]. Specifically, UiO-67(BPY-Me_2) after Pd^{2+} post-metalation exhibited 110-fold and 496-fold enhancement in catalytic activity when compared with Pd complex doped in UiO-67(BPY) and other methyl functionalized of BPY^{2-} supported on UiO-67, respectively [43]. In another case, UiO-67(BPY) loaded with Pd(II) was found as an active recyclable catalyst in aqueous media for carbon–carbon bond formation exemplified by the synthesis of all-carbon quaternary centers via conjugate additions of arylboronic acids to β,β-disubstituted enones. Furthermore, this catalyst could be recycled up to 8 times without loss of crystallinity (yields >75%). In addition, a wide range of functionalities substituted arylboronic acids and β,β-disubstituted enones, can be stereoelectronically catalyzed by UiO-67(BPY)-Pd$(OAc)_2$ in modest-to-high yields (34–95%) [63]. Finally, the MMS strategy has been employed to incorporate Pd(II) in the framework of UiO-67(BPY), in which, the *in-situ* assembly of the mixed linkers consisting of H_2BPY-$PdCl_2$ and H_2BPDC with $ZrCl_4$ metal source was conducted in a non-modulator media to produce the formation of Pd(II)-functionalized UiO-67(BPY). This catalyst was found active for Heck and Suzuki coupling reaction of chloroarenes. Additionally, various kinds of chloroarene substitutes were also utilized as the substrates for use in this reaction with the yield mostly greater than 90% [64]. It should be emphasized that this result significantly differs from those observed by Li et al. [43].

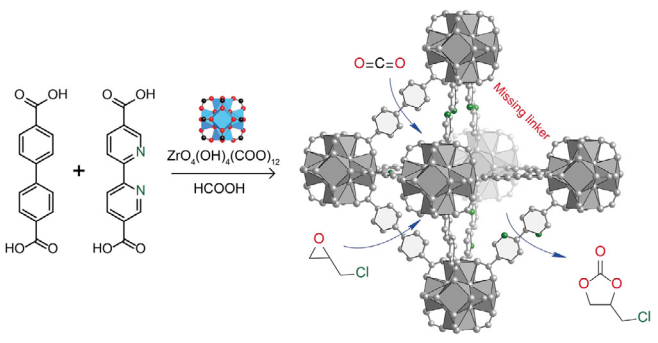

Fig. 12. Coupling reaction of epichlorohydrin with CO_2 using MOF-53.

4.1.6. Catalysis for other transformations

Despite the significant efforts contributed to a specific class of catalysis reaction (*i.e.* CO_2 reduction and hydrogen evolution), there are other important reactions that can be catalyzed by BPY-functionalized Zr-MOFs with anchored active metal centers. Indeed, the distribution of mono-active center onto Zr-MOFs surface or the collaborative interactions among those of active components granted the composites unique properties. Accordingly, anchoring of BPY-$[Ir^{III}(DCPPY)_2]Cl$ and BPY-$[Ru^{II}(BPY)_2]Cl_2$ onto the internal surface of UiO-67(BPY) was found to effectively catalyze photocatalytic transformations of organic substrates in aza-Henry reaction, aerobic amine coupling, and aerobic oxidation of thioanisole with high catalytic activities [31]. Moreover, the post-synthetic metalation of UiO-67(BPY) with $[Ir(COD)(OMe)]_2$ provided Ir-functionalized Zr-MOFs, which were found as highly active catalysts for tandem hydrosilylation of aryl ketones, aldehydes, and dehydrogenative ortho-silylation of benzylicsilyl ethers [58]. Furthermore, Yu and Cohen introduced the UiO-67(BPY) as a photocatalytic material for the hydroxylation of arylboronic acid. In this work, the photocatalytic activity was tested using a photochemical reactor, in which phenylboronic acid, *N*,*N*-diisopropylethylamine, and UiO-67$(BPY)_{0.25}$ were incubated in a methanol solution. This resulted in the conversion of 22% when UV radiation was conducted for 1 day at room temperature. It was concluded that UiO-67$(BPY)_{0.25}$ has the potential to be a photocatalytic material even in mildly basic reactions. However, the conversion was still low and needed improving. Hence, the enhancing photocatalytic performance can be performed by

post-synthetic modification through grafting Ru onto the backbone to cause increasing the conversion up to 81% [65]. Recently, Cohen et al. also reported a single-site catalytic MOF acting as self-propelled micromotors. Accordingly, the MMS strategy was used to synthesize the host framework of UiO-67-$(BPY)_{0.25}$, then the targeted catalyst was obtained by post-metalation of UiO-67-$(BPY)_{0.25}$ with Co^{2+} and Mn^{2+} to produce UiO-67-Co$(BPY)_{0.25}$ and UiO-67-Mn $(BPY)_{0.25}$, respectively. These catalysts were investigated for the decomposition of H_2O_2 to generate oxygen, which triggered the bubble-propelled motion. The propulsion of MOF-nanomotors was tuned by the metal ions, which used to power the micromotor engine. Additionally, a braking system has been designed by adding chelator such as iminodiacetic acid or ethylenediaminetetraacetic acid into the motor-fuel system. Brakes remove the catalytic engine metal ions to further control the speed and motion of micromotors [66].

In another report, a collaborative interaction of the active components was designed via the simple and straightforward protocol of *in situ* incorporation of mono-/bimetal precursors into the framework of Zr-MOFs. This, with the *in-situ* self-assembly of H_2BPY with Zr^{4+} in the presence of a mixture of Pd, Ni metal source, generated the dual Pd, Ni active centers in UiO-67(BPY). Following this, Pd and Ni active centers were then reduced to aggregate into the alloy PdNi NPS constrained within UiO-67(BPY). Due to the collaborative interaction of constrained active catalytic metal sites of Pd and Ni on the surface of PdNi NPs, this composite exhibited superior catalytic activity for the hydrogenation of nitrobenzene as compared with their monometallic counterparts. The synergistic interaction of PdNi NPs with the UiO-67(BPY) backbone was also demonstrated and assigned to explain the better performance in comparison to the monometallic catalyst. It is noted that the higher catalytic performance of this kind of materials was also observed when comparing to the deposited PdNi alloys incorporated on the external surface of Zr-MOFs (Fig. 7). These PdNi nanoparticles in UiO-67(BPY), now termed Pd_7Ni_3@UiO-67(BPY), demonstrated the highest catalytic activity with a quantitative conversion of nitrobenzene to aniline within 3 h under atmospheric pressure of H_2 and 25 °C. It is specifically noticed that Ni-in-UiO-67(BPY) showed no catalytic activity, while Pd@UiO-67 exhibited lower activity compared to Pd_7Ni_3@UiO-67(BPY) [39].

Similarly, the ultrafine bimetallic Pd@Ag core–shell NPs with various Pd/Ag ratios and average sizes of *ca.* 2.6–3.1 nm has been incorporated in the pores of UiO-67(BPY). As a result, the collaborative interaction between the Ag shell and Pd core was immediately recognized to significantly enhance the selectivity in the partial hydrogenation of phenylacetylene at room temperature under atmospheric hydrogen pressure. The resulting investigations indicated improved selectivity (91%) of this bimetallic Pd@Ag core–shell NP as compared with monometallic Pd NPs embedded in UiO-67(BPY) (75% selectivity, >99% phenylacetylene conversion to styrene). On the other hand, Ag NPs embedded in UiO-67(BPY) did not show any catalytic activity. As such, the enhancement in selectivity of the bimetallic Pd@Ag core–shell over the monometallic Pd NPs confined in UiO-67(BPY) was assigned to the synergistic interaction, in which, the Ag shell blocked the high coordination sites of Pd atom at the surface of Pd core [40].

4.2. Molecule adsorption

Guest molecules can be encapsulated inside the pores of MOFs due to their high surface area and large pore volume as well as a high affinity of MOFs framework and adsorbates. In the context of using BPY-functionalized Zr-MOFs, the elegance of design and synthesis allowed this type of material to be coupled with different types of metal complexes, embedded nanoparticles or organic functional groups via *N*-quaternization of the pyridine sites to further enhance the interactive properties of the resulting material and guest molecules compared with the pristine Zr-MOFs (Table 2). For which, Li et al. prepared UiO-67(BPY) to enhance the gas uptake capacities by anchoring Lewis basic sites onto the surface while keeping high porosity and exceptional robustness. As the pore environment of UiO-67(BPY) was populated with N donor atoms, this material exhibited high uptake capacities for H_2, CO_2, and CH_4. The H_2 adsorption capacity, which was found to be 5.7 wt% at 77 K and 20 bar, is 26.6% higher than that of UiO-67 (4.5 wt% at the same conditions). Accordingly, this uptake is among the highest in MOFs used for the purpose of hydrogen storage. The CO_2 and CH_4 uptake capacities were 7.97 wt% and 12.2 wt% (7.63 mmol g^{-1}) at 293 K and 20 bar, respectively. This material ranked among the benchmarks of MOFs for CO_2 capture. Interestingly, these CO_2 uptakes are higher than the experimental or theoretical CO_2 uptake capacities on UiO-67 and UiO-68 [24]. Liang et al. performed experimental and computational studies for CO_2 adsorption performance on Zr-MOFs (MIL-140 series), which was typified by MIL-140A ([ZrO(bdc)], bdc = 1,4-benzenedicarboxylate), and its analogues including H_2BPY linker-based MOFs. It is reported that the CO_2–sorbent interactions were markedly influenced by pore-confinement effects, which arose from a π-stacked arrangement of the ligands within the framework backbone [67].

Nickerl et al. prepared UiO-67(BPY) and the BPY building unit was then functionalized by post-synthetic metalation with different metal salts ($M^{II}X_y$; M = Cu^{2+}, Ni^{2+}, Co^{2+}; X = Cl^-, NO_3^-, SO_4^{2-}, $acac^{2-}$ = acetylacetonate) by soaking the MOF in aqueous or ethanolic solution, containing 2 equivalents per linker metal salt to produce the corresponding metal@UiO-67(BPY) materials. The series of metalated materials was investigated for their hydrogen

Table 2
Applications of functionalized UiO-67(BPY) in molecule adsorption.

No.	Material	Active centers	Applications	Result	Refs.
1	UiO-67(BPY)	BPY	Uptake of H_2, CO_2 and CH_4	-H_2 adsorption capacity of UiO-67(BPY) was 5.7 wt% at 77 K and 20 bar. -The CO_2 and CH_4 uptake capacities were 7.97 wt% and 12.2 wt% (7.63 mmol g^{-1}), at 293 K and 20 bar.	[24]
2	Metal_salt@UiO-67(BPY)	BPY-MX M: Cu^{2+}, Co^{2+}, Ni^{2+} X: Cl^-, SO_4^{2-}, NO_3^-, $acac^{2-}$	Removal of H_2S	The copper loaded samples have the highest capture capacity up to 7.8 wt% (H_2S).	[28]
3	MOF-867 ZJU-101	Methyl function of N-chelation sites of BPY^{2-} linker	$Cr_2O_7^{2-}$ removal in water	ZJU-101 exhibited $Cr_2O_7^{2-}$ uptake of 245 mg g^{-1} with high adsorption selectivity.	[33]
4	UiO-67-BPY UiO-67-BPY-Me	Methyl function of N donor sites of BPY^{2-} linker	Anionic dye adsorption MO (methyl orange)	UiO-67-BPY-Me is more efficient in catalyzing degradation of MO under UV-vis light irradiation.	[34]
5	MIL-140C-25	BPDC and BPY	CO_2 uptake	The highest CO_2 uptake is up 19.6% at 1.2 bar and 293 K with MIL-140C-25.	[67]
6	ZJU-101	BPY	Drug loading (diclofenac sodium)	The loading capacity of the MOF is ~ 0.546 g g^{-1}.	[68]

sulfide (H_2S) and ammonia adsorption properties. The results indicated that metal@UiO-67(BPY) materials exhibit good performance in toxic hydrogen sulfide capture. Especially, the copper-loading samples have high capacities up to 7.8 wt%, while no specific affinity towards hydrogen sulfide was observed for UiO-67 and UiO-67 (BPY). This advancement in hydrogen sulfide capture was attributed to the highly dispersed metal ions onto the surface of metal@UiO-67(BPY). Furthermore, as metal@UiO-67(BPY) maintained the crystallinity as well as porosity after hydrogen sulfide uptake, it suggested the real chance for these materials to use in the practical applications such as petroleum-related field [28].

Another synthetic strategy for the modification of UiO-67(BPY) was reported, in which, UiO-67(BPY) were post-modified via *N*-quaternization of the pyridine sites to form UiO-67-BPY-Me and UiO-67-BPY-Me_2, respectively. Both of those materials contained the cationic framework whose thermal and chemical stabilities were primarily preserved. Interestingly, the existence of cationic centers in UiO-67-BPY-Me facilitated fast anionic dye adsorption [34]. Furthermore, dimethylated cationic form (UiO-67-BPY-Me_2) was found as a highly efficient material for $Cr_2O_7^{2-}$ removal from water [33]. Additionally, UiO-67-BPY-Me_2 (ZJU-101) could perform as a drug carrier for loading of diclofenac sodium. The mechanism of the drug carrier was assigned to the anion exchange between anions in phosphate buffered saline (PBS) and coordinated/free diclofenac anions. Experimental results displayed the maximum loading capacity of ~0.546 g g^{-1} of diclofenac sodium inside the MOF's structure. Furthermore, UiO-67-BPY-Me_2 also demonstrated a physiological pH-responsive drug release (the drug release in PBS of pH = 5.4 is faster than in PBS of pH = 7.4) [68].

Additionally, as the molecule adsorption depends on the concentration of adsorbates and temperature, we believe that future directions will focus on the design and synthesis of synergistic systems, which are composed of specific active components for the indirect control of adsorbed factors such as the local temperature at adsorbed sites, to allow the smart release or adsorption of guest molecules. For example, the release of guest molecules (gases, drugs) can be controlled by exploiting the plasmonic effect of embedded Ag nanoparticle in BPY-functionalized Zr-MOFs. Aside from our suggestions, the controlled release of Ag^+ ions, which were loaded in the Zr-MOFs UiO-67(BPY) and UiO-66-$(COOH)_2$, was demonstrated by Hmadeh et al. via changing the functional groups of the linker very recently [69].

4.3. Luminescence sensor

As discussed in previous sections, the high surface area and large pore volume of UiO-67(BPY) allows for the accommodation of guest molecules inside its pores. Additionally, UiO-67(BPY) possesses luminescence emitting centers from the BPY group providing the unique opportunity for the materials to be utilized as sensors, in which the alternation on luminescence signal can be observed as guest molecules adsorbed in the pores (Table 3). An example for a guest-dependent luminescence sensor, which employed UiO-67(BPY) as the platform, was the utilization of this material for metal detection based on the binding sites of BPY functional groups that can interact with free metal ions in the solution via chelation. In this system, BPY^{2-} linker served as the chelator for ion pre-concentration as well as the fluorescent reporter for signal detection. Interestingly, this MOF sensor was found to detect Fe^{3+} with the threshold of 3.2 ppb. Furthermore, a broad range of metal ion (Mn^{2+}, Fe^{2+}, Co^{2+}, Ni^{2+}, Cu^{2+}, Zn^{2+}, Cd^{2+}) was found to be effectively detected by this sensor [70]. The luminescence of UiO-67 (BPY) can be alternated via partial chelation of BPY centers with Eu^{3+} luminescence metal ions to generate the synergistic interaction of the system composed of dual-emitting sites. This further triggered the ratiometric dependence of luminescence come from the effect of the dual-emitting sites on temperature. Furthermore, this phenomenon was attributed to the back-energy transfer (BEnT) from Eu^{3+} cations to BPY^{2-} linkers and, according to the authors, this material can be used for highly sensitive temperature sensing [71]

In another example, UiO-67(BPY), after chelating with Eu^{3+} ion, was employed as a guest-dependent luminescence sensor to recognize volatile organic compounds. Accordingly, this sensor was used for the recognition of aromatic volatile organic compounds (VOCs), in which the dual-readout signal, combined ratiometric emission intensity and luminescence quantum yield, has been highlighted to recognize aromatic VOCs (benzene, toluene, *o*-xylene, *m*-xylene, *p*-xylene, ethylbenzene, chlorobenzene, and benzonitrile). This further gave 2D decoded maps of these molecules based on the emission intensity ratio (I_L/I_{Eu}) and quantum yield (Φ) responses of the host platform towards the accommodation [72].

Different from other examples, Liu et al. prepared a biodegradable and biocompatible contrast agent for *in vitro* optical imaging. Accordingly, the system design consisted of the BPY-based Zr-MOF, which was formulated from the reaction of phosphorescent Ru-$H_2BPY(bpy)_2$ complex (bpy = 2,2′-bipyridine) and $ZrCl_4$ in DMF via microwave-assisted irradiation [73]. The water stability of the Ru-functionalized BPY-based Zr-MOF increased, but it rapidly decomposed in phosphate-buffered saline solution due to the reaction between Zr and phosphates. Following this, silica was coated as a thin shell around the MOF to increase the stability. This system was then post-modified by polyethylene glycol (PEG), which, via the interaction with silanol groups of silica, was attached to the surface of silica coated MOF to form PEG-SiO_2@Zr-MOF composite. In the next step of the synthesis, this composite was treated with anisamide (AA) to form AA-PEG-SiO_2@Zr-MOF. Coating a polyethylene glycol (PEG) layer was performed in order to prevent particles from aggregation in AA. Finally, the obtained composites, PEG-SiO_2@Zr-MOF and AA-PEG-SiO_2@Zr-MOF, were grafted onto tumor targeting to test for their *in vitro* viability assays on H460 non-small cell lung cancer cells. As expected, laser scanning confo-

Table 3
Applications of functionalized UiO-67(BPY) as luminescence sensor.

No.	Material	Active centers	Applications	Result	Refs.
1	UiO-67-BPY	BPY	Luminescence sensor for detection of metals ion	MOF sensor was excellently found to detect Fe^{3+} with a detection limit of 3.2 ppb and other metal ions.	[70]
2	Eu^{3+}@UiO-BPY	BPY-$EuCl_3$	Temperature sensor	The highest thermometric sensitivity is 2.99% K^{-1}.	[71]
3	Eu^{3+}@UiO-BPY	BPY-$EuCl_3$	The recognition of aromatic VOCs (volatile organic compounds)	Ratiometric emission intensity and luminescence quantum yield was highlighted to recognized aromatic VOCs.	[72]
4	NCP-2 PEG-SiO_2@2 AA-PEG-SiO_2@2	[{5,5′-$(CO_2H)_2$-BPY}$(BPY)_2$]$(PF_6)_2$	Optical imaging	Luminescent hybrid nanoparticles were synthesized by nanoscale polymers with extremely high dye loadings for optical imaging.	[73]

Table 4
Applications of functionalized UiO-67(BPY) in solar cell applications.

No.	Material	Active centers	Applications	Result	Refs.
1	Zr:Cu MOF	BPY-CuI	Solar cell	Improving the stability of the prepared $Cu_{2-x}S$/CdS PV cells after the first 10 d.	[26]
2	UiO-67-Ru-DCBPY	$[BPY\text{-}Ru(BPY_m)_2]Cl_2$	Solar cell	The efficiencies of the cells are less than 1%, MOFSCs can present a promising platform for photovoltaic applications as compared to traditional materials.	[74]

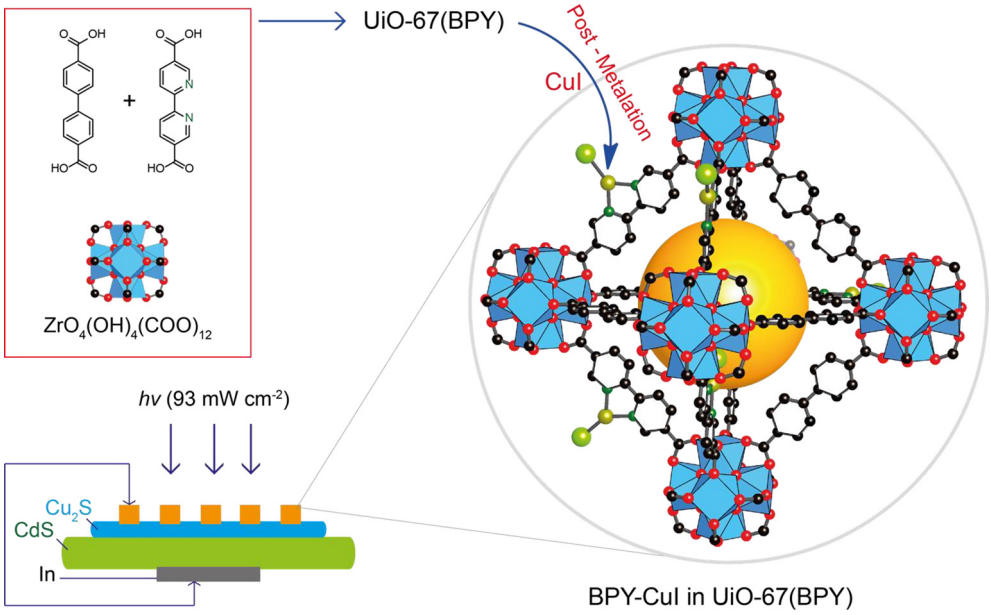

Fig. 13. Synthesis of UiO-67(BPY)-CuI and its application in $Cu_{2-x}S$/CdS PV cells as the copper compensated source for diffused copper ions out from Cu_2S layer.

Table 5
Applications of functionalized UiO-67(BPY) in others.

No.	Material	Active centers	Applications	Result	Refs.
1	nMOF-867	BPY	Supercapacitor	Area capacitance of 0.64 and 5.09 mF cm^2.	[75]
2	Li-polysulphides@nMOF-867	BPY	Lithium battery	Over 500 discharge/charge cycles. Discharge capacity of 788 mAh g^{-1} at a high current rate of 835 mA g^{-1}.	[76]

cal fluorescence microscopy studies showed relatively strong luminescence for AA-PEG-SiO_2@Zr-MOF as opposed to PEG-SiO_2@Zr-MOF. This result indicates that the BPY-functionalized Zr-MOF platform can be utilized as an alternative to replace toxic contrast agents.

4.4. Solar cell applications

Owing to global environmental issues and increasing demand for alternative and clean energy, utilization of solar energy is required, however, the photovoltaics are needed to convert solar energy into electric energy. Recently, MOFs have been reported for solar cells applications (Table 4). Cu_2S-based photovoltaics solar cells represent a cost-effective technique; however, this has suffered from rapid performance degradation due to the diffusion of copper ions into the CdS layer. To prevent this performance degradation, Nevruzoglu et al. prepared CuI-loaded UiO-67(BPY), which contained $BPDC^{2-}$ and BPY^{2-} (50%), to capture copper ions (Fig. 13). This material was subsequently used for the compensation of the diffused copper ions into the CdS layer which, as a result, improved the stability of the prepared $Cu_{2-x}S$/CdS PV cells for at least 40 days [26]. Apart from chalcogenide solar cells, MOF-sensitized solar cells (MOFSCs) were reported by Maza et al. Accordingly, photo-sensitized $BPY\text{-}Ru(II)(BPY_m)_2$ complex was incorporated into UiO-67(BPY) thin films via three different methods to obtain MOFSCs, which were subsequently used as sensitizing materials on TiO_2 for solar cell applications. The prepared system successively generated photocurrent in response to simulated 1-day sun illumination. The efficiencies of the cells were less than 1%, however, MOFSCs can be considered as a promising platform for photovoltaic applications [74]

4.5. Energy storage

Despite their long-life cycle, the employment of carbon-based supercapacitors as energy storage devices suffers from low capacitance, in addition to the challenges of preparing a supercapacitor with high capacitance and high life cycle. Recently, MOFs have been used for energy storage and conversion, including fuel storage, hydrogen evolution, solar cells, fuel cells, batteries, and supercapacitors (Table 5). In this context, UiO-67(BPY) has been considered as a promising material for supercapacitor application. Choi et al. succeeded to prepare a hybrid device using a mixture of UiO-67(BPY) and graphene. In this work, UiO-67(BPY) was doped with graphene and incorporated into the devices to construct the supercapacitors. Accordingly, UiO-67(BPY) has a stack and areal

capacitance of 0.64 and 5.09 mF cm^2, respectively, which was about 6 times higher than that of the supercapacitors made from the benchmark commercial activated carbon materials and the performance period was preserved over at least 10,000 charge/discharge cycles [75]

Development of high-performance energy storage device with stable life cycles and high energy density is challenging. Hence, design of the lithium-sulphur (Li-S) batteries, which has a high theoretical energy density, has attracted attention. Indeed, the dissolution of lithium polysulphides, generated during discharge in the cathode of a Li-S battery, shortens the life cycle of the battery. Park et al. demonstrated via *in situ* spectroelectrochemical measurements that the sp^2 nitrogen atoms in the organic linkers of nanocrystalline UiO-67(BPY) (nMOF-867) were able to encapsulate lithium polysulphides inside the microcages of nMOF-867, thus helping to prevent their dissolution into the electrolyte during discharge/charge cycles. As a result, the nMOF-867 containing cathode exhibited excellent capacity retention over the long life of 500 discharge/charge cycles with the capacity loss of approximately 0.027% per cycle from a discharge capacity of 788 mAh/g at a high current rate of 835 mA/g [76].

5. Conclusion and future perspectives

In conclusion, BPY-functionalized Zr-MOFs, with the flexibility in design and synthesis as well as viable post-modification pathways, facilitate tailorable features with the synergistic combination of properties, which arises from the interactions between active components and the host framework. Hence, in this review, the synthetic strategies, characterization methods have been comprehensively summarized. We further highlighted the novel practical applications by exploiting the UiO-based catalytic platforms. In this context, the detailed discussion and our viewpoint for developing new catalytic systems containing exceptional performance caused by the synergistic interactions between the metal active constituent and MOFs framework were also presented. Based on the naturally tunable and designable properties of MOFs structures, we believe that the systems of BPY-functionalized Zr-MOFs, and those with similar properties can be pre-designed with higher levels of synergistic interactions, synthesized, and employed for particular applications. Furthermore, the incorporation of multiple active metal centers within BPY-functionalized Zr-MOFs in a specific order can be aimed for synthesis via the combined method of the step-by-step and layer-by-layer growth of an organic–inorganic layer onto the substrate [6]. Consequently, the strategies summarized in this review such as PSE, linker exchange, and MMS, along with characterization methods can be adaptable to other related MOFs like hafnium (Hf) or cerium (Ce)-BPY. This can provide new opportunities for the synthesis of advanced materials with diverse topologies and we believe that this review has provided the basis for paving the way towards inspiring researchers to design better and more efficient systems for specific applications.

Competing interests

All authors declare no competing interests.

Acknowledgements

We thank Prof. Omar M. Yaghi (University of California, Berkeley) for his support of global science efforts. S.D. gratefully acknowledges the Scientific and Technological Research Council of Turkey, (TÜBİTAK) (No. 112T956) for their support. T.N.T. and M.V.N. are supported by the U.S. Office of Naval Research Global: Naval International Cooperative Opportunities in Science and Technology Program (No. N62909-16-1-2146). K.E.C. and H.L.N. would like to acknowledge Saudi Aramco (ORCP2390) for their continued collaboration and support. K.E.C. and B.Y. acknowledge the World Class Professor (WCP) Grant, Ministry of Research, Technology and Higher Education, Republic of Indonesia.

References

[1] H. Furukawa, K.E. Cordova, M. O'Keeffe, O.M. Yaghi, Science 341 (2013) 1230444.
[2] K. Adil, Y. Belmabkhout, R.S. Pillai, A. Cadiau, P.M. Bhatt, A.H. Assen, G. Maurin, M. Eddaoudi, Chem. Soc. Rev. 46 (2017) 3402–3430.
[3] F. Gándara, H. Furukawa, S. Lee, O.M. Yaghi, J. Am. Chem. Soc. 136 (2014) 5271–5274.
[4] J. Liu, L. Chen, H. Cui, J. Zhang, L. Zhang, C.-Y. Su, Chem. Soc. Rev. 43 (2014) 6011–6061.
[5] P. Horcajada, P. Gref, T. Baati, P.K. Allan, G. Maurin, P. Couvreur, G. Férey, R.E. Morris, C. Serre, Chem. Rev. 112 (2012) 1232–1268.
[6] X. Meng, H.N. Wang, S.-Y. Song, H.-J. Zhang, Chem. Soc. Rev. 46 (2017) 464–480.
[7] T.N. Tu, N.Q. Phan, T.T. Vu, H.L. Nguyen, K.E. Cordova, H. Furukawa, J. Mater. Chem. A 4 (2016) 3638–3641.
[8] L.E. Kreno, K. Leong, O.K. Farha, M. Allendorf, R.P.D. Van, J.T. Hupp, Chem. Rev. 112 (2012) 1105–1125.
[9] A.J. Howarth, Y. Liu, P. Li, Z. Li, T.C. Wang, J.T. Hupp, O.K. Farha, Nat. Rev. Mater. 1 (2016) 15018.
[10] J. Canivet, A. Fateeva, Y. Guo, B. Coasne, D. Farrusseng, Chem. Soc. Rev. 43 (2014) 5594–5617.
[11] J.B. DeCoste, G.W. Peterson, H. Jasuja, T.G. Glover, Y. Huang, K.S. Walton, J. Mater. Chem. A 1 (2013) 5642–5650.
[12] J.H. Cavka, S. Jakobsen, U. Olsbye, N. Guillou, C. Lamberti, S. Bordiga, K.P. Lillerud, J. Am. Chem. Soc. 130 (2008) 13850–13851.
[13] Y. Bai, Y. Dou, L.H. Xie, W. Rutledge, J.R. Li, H.C. Zhou, Chem. Soc. Rev. 45 (2016) 2327–2367.
[14] H. Wu, Y.S. Chua, V. Krungleviciute, M. Tyagi, P. Chen, T. Yildirim, W. Zhou, J. Am. Chem. Soc. 135 (2013) 10525–10532.
[15] G. Wißmann, A. Schaate, S. Lilienthal, I. Bremer, A.M. Schneider, P. Behrens, Microporous Mesoporous Mater. 152 (2012) 64–70.
[16] H. Furukawa, F. Gándara, Y.B. Zhang, J. Jiang, W.L. Queen, M.R. Hudson, O.M. Yaghi, J. Am. Chem. Soc. 136 (2014) 4369–4381.
[17] O.V. Gutov, M.G. Hevia, E.C. Escudero-Adán, A. Shafir, Inorg. Chem. 54 (2015) 8396–8400.
[18] W. Morris, B. Volosskiy, S. Demir, F. Gándara, P.L. McGrier, H. Furukawa, D. Cascio, J.F. Stoddart, O.M. Yaghi, Inorg. Chem. 12 (2012) 6443–6445.
[19] D. Feng, W.C. Chung, Z. Wei, Z.Y. Gu, H.L. Jiang, Y.P. Chen, D.J. Darensbourg, H.C. Zhou, J. Am. Chem. Soc. 135 (2013) 17105–17110.
[20] D. Feng, Z.Y. Gu, Y.P. Chen, J. Park, Z. Wei, Y. Sun, M. Bosch, S. Yuan, H.C. Zhou, J. Am. Chem. Soc. 136 (2014) 17714–17717.
[21] T.H.N. Lo, M.V. Nguyen, T.N. Tu, Inorg. Chem. Front. 4 (2017) 1509–1516.
[22] M.V. Nguyen, T.H.N. Lo, L.C. Luu, H.T.T. Nguyen, T.N. Tu, J. Mater. Chem. A 6 (2018) 1816–1821.
[23] D. Alezi, I. Spanopoulos, C. Tsangarakis, A. Shkurenko, K. Adil, Y. Belmabkhout, M. O'Keeffe, M. Eddaoudi, P.N. Trikalitis, J. Am. Chem. Soc. 138 (2016) 12767–12770.
[24] L. Li, S. Tang, C. Wang, X. Lv, M. Jiang, H. Wu, X. Zhao, Chem. Commun. 50 (2014) 2304–2307.
[25] Y. Kim, S. Huh, CrystEngComm 18 (2016) 3524–3550.
[26] V. Nevruzoglu, S. Demir, G. Karaca, M. Tomakin, N. Bilgin, F. Yilmaz, J. Mater. Chem. A 4 (2016) 7930–7935.
[27] A. Schaate, P. Roy, A. Godt, J. Lippke, F. Waltz, M. Wiebcke, P. Behrens, Chem. Eur. J. 24 (2011) 6643–6651.
[28] G. Nickerl, M. Leistner, S. Helten, V. Bon, I. Senkovska, S. Kaskel, Inorg. Chem. Front. 1 (2014) 325–330.
[29] H. Fei, S.M. Cohen, Chem. Commun. 50 (2014) 4810–4812.
[30] O. Karagiaridi, W. Bury, J.E. Mondloch, J.T. Hupp, O.K. Farha, Angew. Chem. Int. Ed. 53 (2014) 4530–4540.
[31] C. Wang, Z. Xie, K.E. DeKrafft, W. Lin, J. Am. Chem. Soc. 133 (2011) 13445–13454.
[32] M.I. Gonzalez, E.D. Bloch, J.A. Mason, S.J. Teat, J.R. Long, Inorg. Chem. 54 (2015) 2995–3005.
[33] Q. Zhang, J. Yu, J. Cai, L. Zhang, Y. Cui, Y. Yang, B. Chen, G. Qian, Chem. Commun. 51 (2015) 14732–14734.
[34] L. Xu, Y. Luo, L. Sun, S. Pu, M. Fang, R.X. Yuan, H.B. Du, Dalton Trans. 45 (2016) 8614–8621.
[35] K. Manna, T. Zhang, F.X. Greene, W. Lin, K. Manna, T. Zhang, F.X. Greene, W. Lin, J. Am. Chem. Soc. 137 (2015) 2665–2673.
[36] C.C. Hou, T.T. Li, S. Cao, Y. Chen, W.F. Fu, J. Mater. Chem. A 3 (2015) 10386–10394.
[37] D. Kim, D.R. Whang, S.Y. Park, J. Am. Chem. Soc. 138 (2016) 8698–8701.
[38] A.E. Platero-Prats, A.B. Gómez, L. Samain, X. Zou, B. Martín-Matute, Chem. Eur. J. 21 (2015) 861–866.
[39] L. Chen, X. Chen, H. Liu, Y. Li, Small 11 (2015) 2642–2648.

[40] L. Chen, B. Huang, X. Qiu, X. Wang, R. Luque, Y. Li, Chem. Sci. 7 (2016) 228–233.
[41] K.M. Choi, K. Na, G.A. Somorjai, O.M. Yaghi, J. Am. Chem. Soc. 137 (2015) 7810–7816.
[42] C. Wang, K.E. Dekrafft, W. Lin, J. Am. Chem. Soc. 134 (2012) 7211–7214.
[43] X. Li, R. Van Zeeland, R.V. Maligal-Ganesh, Y. Pei, G. Power, L. Stanley, W. Huang, ACS Catal. 6 (2016) 6324–6328.
[44] S. Øien, G. Agostini, S. Svelle, E. Borfecchia, K.A. Lomachenko, L. Mino, E. Gallo, S. Bordiga, U. Olsbye, K.P. Lillerud, C. Lamberti, Chem. Mater. 27 (2015) 1042–1056.
[45] L. Braglia, E. Borfecchia, L. Maddalena, S. Øien, K.A. Lomachenko, A.L. Bugaev, S. Bordiga, A.V. Soldatov, K.P. Lillerud, C. Lamberti, Catal. Today 283 (2017) 89–103.
[46] C.H. Hendon, J. Bonnefoy, E.A. Quadrelli, J. Canivet, M.B. Chambers, G. Rousse, A. Walsh, M. Fontecave, C. Mellot-Draznieks, Chem. Eur. J. 22 (2016) 3713–3718.
[47] W.A. Maza, S.R. Ahrenholtz, C.C. Epley, C.S. Day, A.J. Morris, J. Phys. Chem. C 118 (2014) 14200–14210.
[48] W.A. Maza, R. Padilla, A.J. Morris, J. Am. Chem. Soc. 137 (2015) 8161–8168.
[49] M.H. Beyzavi, C.J. Stephenson, Y. Liu, O. Karagiaridi, J.T. Hupp, O.K. Farha, Front. Energy Res. 2 (2015) 1–10.
[50] S.M. Cohen, Z. Zhang, J.A. Boissonnault, Inorg. Chem. 55 (2016) 7281–7290.
[51] J. Wang, C. Wang, W. Lin, ACS Catal. 2 (2012) 2630–2640.
[52] A. Dhakshinamoorthy, A.M. Asiri Garcia, Catal. Sci. Technol. 6 (2016) 5238–5261.
[53] M. Rimoldi, A.J. Howarth, M.R. DeStefano, L. Lin, S. Goswami, P. Li, J.T. Hupp, O. K. Farha, ACS Catal. 7 (2017) 997–1014.
[54] T. Kajiwara, M.H. Fujii, M. Tsujimoto, K. Kobayashi, M. Higuchi, K. Tanaka, S. Kitagawa, Angew. Chem. Int. Ed. 55 (2016) 2697–2700.
[55] H. Fei, M.D. Sampson, Y. Lee, C.P. Kubiak, S.M. Cohen, Inorg. Chem. 54 (2015) 6821–6828.
[56] K.M. Choi, D. Kim, B. Rungtaweevoranit, C.A. Trickett, J.T.D. Barmanbek, A.S. Alshammari, P. Yang, O.M. Yaghi, J. Am. Chem. Soc. 139 (2017) 356–362.
[57] T. Toyao, M. Saito, S. Dohshi, K. Mochizuki, M. Iwata, H. Higashimura, Y. Horiuchi, M. Matsuoka, Res. Chem. Intermed. 42 (2016) 7679–7688.
[58] K. Manna, T. Zhang, W. Lin, J. Am. Chem. Soc. 136 (2014) 6566–6569.
[59] T. Zhang, K. Manna, W. Lin, J. Am. Chem. Soc. 138 (2016) 3241–3249.
[60] P. Neves, A.C. Gomes, T.R. Amarante, F.A.A. Paz, M. Pillinger, I.S. Gonçalves, A.A. Valente, Microporous Mesoporous Mater. 202 (2015) 106–114.
[61] T. Toyao, K. Miyahara, M. Fujiwaki, T.H. Kim, S. Dohshi, Y. Horiuchi, M. Matsuoka, J. Phys. Chem. C 119 (2015) 8131–8137.
[62] S. Demir, S. Usta, H. Tamar, M. Ulusoy, Microporous Mesoporous Mater. 244 (2017) 251–257.
[63] R. Van Zeeland, X. Li, W. Huang, L.M. Stanley, RSC Adv. 6 (2016) 56330–56334.
[64] L. Chen, S. Rangan, J. Li, H. Jiang, Y. Li, Green Chem. 16 (2014) 3978–3985.
[65] X. Yu, S.M. Cohen, Chem. Commun. 15 (2015) 9880–9883.
[66] J. Li, X. Yu, M. Xu, W. Liu, E. Sandraz, H. Lan, J. Wang, S.M. Cohen, J. Am. Chem. Soc. 139 (2017) 611–614.
[67] W. Liang, R. Babarao, T.L. Church, D.M. D'Alessandro, Chem. Commun. 51 (2015) 11286–11289.
[68] Y. Yang, Q. Hu, Q. Zhang, K. Jiang, W. Lin, Y. Yang, Y. Cui, G. Qian, Mol. Pharm. 13 (2016) 2782–2786.
[69] B. Mortada, T.A. Matar, A. Sakaya, H. Atallah, Z.K. Ali, P. Karam, M. Hmadeh, Inorg. Chem. 56 (2017) 4739–4744.
[70] X. Lin, Y. Hong, C. Zhang, R. Huang, C. Wang, W. Lin, Chem. Commun. 51 (2015) 16996–16999.
[71] Y. Zhou, B. Yan, J. Mater. Chem. C 3 (2015) 9353–9358.
[72] Y. Zhou, B. Yan, Chem. Commun. 52 (2015) 2265–2268.
[73] D. Liu, R.C. Huxford, W. Lin, Angew. Chem. Int. Ed. 50 (2011) 3696–3700.
[74] W.A. Maza, A.J. Haring, S.R. Ahrenholtz, C.C. Epley, S.Y. Lin, A.J. Morris, Chem. Sci. 7 (2016) 719–727.
[75] K.M. Choi, H.M. Jeong, J.H. Park, Y. Zhang, J.K. Kang, ACS Nano 8 (2014) 7451–7457.
[76] J.H. Park, K.M. Choi, D.K. Lee, B.C. Moon, S.R. Shin, M.K. Song, J.K. Kang, Sci. Rep. 6 (2016) 25555.